



**FORECASTING ADVECTIVE SEA FOG WITH THE USE OF
CLASSIFICATION AND REGRESSION TREE ANALYSES FOR
KUNSAN AIR BASE**

THESIS

Danielle M. Lewis, Captain, USAF

AFIT/GM/ENP/04-08

**DEPARTMENT OF THE AIR FORCE
AIR UNIVERSITY**

AIR FORCE INSTITUTE OF TECHNOLOGY

Wright-Patterson Air Force Base, Ohio

APPROVED FOR PUBLIC RELEASE; DISTRIBUTION UNLIMITED

The views expressed in this thesis are those of the author and do not reflect the official policy or position of the United States Air Force, Department of Defense, or the United States Government.

FORECASTING ADVECTIVE SEA FOG WITH THE USE OF
CLASSIFICATION AND REGRESSION TREE ANALYSES FOR
KUNSAN AIR BASE

THESIS

Presented to the Faculty

Department of Engineering Physics

Graduate School of Engineering and Management

Air Force Institute of Technology

Air University

Air Education and Training Command

In Partial Fulfillment of the Requirements for the

Degree of Master of Science in Meteorology

Danielle M. Lewis, BS

Captain, USAF

March 2004

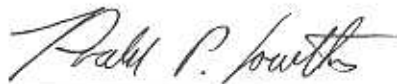
APPROVED FOR PUBLIC RELEASE; DISTRIBUTION UNLIMITED

AFIT/GM/ENP/04-08

FORECASTING ADVECTIVE SEA FOG WITH THE USE OF
CLASSIFICATION AND REGRESSION TREE ANALYSES FOR
KUNSAN AIR BASE

Danielle M. Lewis, BS
Captain, USAF

Approved:



Ronald P. Lowther (Chairman)

8 MAR 04

date



Michael K. Walters (Member)

9 MAR 04

date



Daniel F. Reynolds (Member)

9 Mar 04

date

Abstract

Advection sea fog frequently plagues Kunsan Air Base (AB), Republic of Korea, in the spring and summer seasons. It is responsible for a variety of impacts on military operations, the greatest being to aviation. To date, there are no suitable methods developed for forecasting advection sea fog at Kunsan, primarily due to a lack of understanding of sea fog formation under various synoptic situations over the Yellow Sea. This work explored the feasibility of predicting sea fog development with a 24-hour forecast lead time. Before exploratory data analysis was performed, a geographical introduction to the region was provided along with a discussion of basic elements of fog formation, the physical properties of fog droplets, and its dissipation.

Examined in this work were data sets of Kunsan surface observations, upstream upper air data, sea surface temperatures over the Yellow Sea, and modeled analyses of gridded data over the Yellow Sea. A complete ten year period of record was examined for inclusion into data mining models to find predictive patterns. The data were first examined using logistic regression techniques, followed by classification and regression tree analysis (CART) for exploring possible concealed predictors. Regression revealed weak relationships between the target variable (sea fog) and upper air predictors, with stronger relationships between the target variable and sea surface temperatures. CART results determined the importance between the target variable and upstream upper air predictors, and established specific criteria to be used when forecasting target variable events. The results of the regression and CART data mining analyses are summarized as forecasting guidelines to aid forecasters in predicting the evolution of sea fog events and advection over the area.

Acknowledgments

I would like to thank many people who made this research possible. First, I would like to thank my thesis advisor, Lt Col Ronald Lowther, for his guidance and mentorship throughout this project. I would also like to express my gratitude to my other committee members, Lt Col Michael Walters and Mr. Daniel Reynolds for the expertise they provided.

I would like to thank the staff at the Air Force Combat Climatology Center and the Air Force Weather Library in Asheville, North Carolina for providing me with all the data and research materials I needed to complete this project. Additionally, I would like to thank my sponsor at the 8th Operational Support Squadron Weather Flight at Kunsan Air Base, Korea, for providing the funding necessary to accomplish this task.

Next I would like to thank my classmates, particularly Captains Jonathan Leffler, Kevin Bartlett, Scott Miller, and Lou Lussier. Without their help and tips, I would most likely still be formatting my data.

And finally, I would like to thank my family for supporting me in all my endeavors. I would not have made it this far without them.

Danielle M. Lewis

Table of Contents

	Page
Abstract	iv
Acknowledgments	v
List of Figures	viii
List of Tables	x
I. Introduction	1
Statement of the Problem.....	1
Scope of Research.....	2
Research Objectives.....	4
II. Background and Literature Review	7
Background.....	7
Fog Formation.....	8
Physical Properties of Sea Fog	19
Dissipation	22
III. Data Collection and Review	24
Data Collection	24
Kunsan AB, ROK Weather Observations.....	24
Sea Surface Temperature (SST) Data.....	25
Upper Air Data.....	27
Data Limitations	30
IV. Methodology.....	31
Data Examination.....	32
Surface Observation Database	32
NOGAPS Upper Air Data.....	33
SST Data	34
Results.....	35
Statistical Analysis.....	35
Logistical Regression.....	36
Logistical Regression Results.....	36

	Page
V. CART Overview, Method, and Results	42
CART Overview	42
Tree Splitting Methods	43
Priors	45
Pruning Trees	46
Testing	46
Cross Validation	46
Fraction of Cases selected at Random for Testing	47
Class Assignment.....	47
CART Methodology and Results.....	48
Initial Classification Testing.....	49
Testing with the Removal of 0° through 135° NOGAPS Winds.....	52
Reclassified Sea Fog Target Variable.....	62
Addition of new predictor variables	71
VI. Conclusion and Recommendations.....	77
Conclusions.....	77
Recommendations.....	80
Appendix A. Decision Tree One for Forecasting Sea Fog at Kunsan AB	82
Appendix B. Decision Tree Two for Forecasting Sea Fog at Kunsan AB	83
Appendix C. Land/Sea Breeze Front Checklist.....	84
Acronyms.....	85
Bibliography	87
Vita.....	90

List of Figures

Figure	Page
1. Map of South Korea.....	7
2. Ocean currents surrounding the Korean Peninsula for (a) Winter (b) Summer.....	9
3. Percentage of fog, January.....	14
4. Percentage of fog, April.....	14
5. Percentage of fog, July.....	15
6. Percentage of fog, October	15
7. Mean sea surface temperature in (a) Dec and (b) Jun.....	17
8. Mean frequency day of sea fog occurrence for (a) Jan and (b) Jul.....	18
9. Relation between visibility and relative humidity at Los Angeles Airport	20
10. Number of fog drops in relation to their diameter	21
11. Polar stereographic grid for RTNEPH model.....	26
12. Sample of instrument errors.....	28
13. NOGAPS grid points used in this study	29
14. Forecast decision tree using Gini, 10-fold cross-validation	53
15. Forecast decision tree using Gini, random sampling.....	54-55
16. Wind circle diagram.....	56
17. Forecast decision tree for Test 2, 10-fold cross-validation.....	58
18. Predictor variables used for splitting Test 2 data with 10-fold cross-validation	60

19. Pruned forecast decision tree from Test 2 data using 10-fold cross validation	61
20. Forecast decision tree produces from Test 3 data, 10-fold cross-validation	64-65
21. Forecast decision tree from Test 4 data, 10-fold cross-validation.....	67
22. Predictor variables used for splitting Test 4 data with 10-fold cross-validation	69
23. Forecast decision tree from pruned Test 4 data, 10-fold cross-validation.....	70
24. Forecast decision tree with AT-SST and DP-SST predictor variables.....	72
25. Forecast decision tree splitters with new predictor variables	74
26. Forecast decision tree with AT-SST and DP-SST predictor variables.....	75

List of Tables

Table	Page
1. Percent frequency of ceiling/visibility less than 3000 feet/3 statute miles.....	31
2. Predictor variables used in JMP.....	38
3. JMP results for Grid Point A	38
4. JMP results for Grid Point B.....	39
5. JMP results for Grid Point C.....	39
6. JMP results for Grid Point D	40
7. Results from stepwise logistic regression performed on JMP	41
8. List of predictor variables used for CART	50
9. Initial relative cost comparison for Grid B data set.....	50
10. 10-fold cross-validation misclassification rates for Grid B data set.....	50
11. Random sampling misclassification rates for Grid B data set	51
12. Relative cost comparison for Test 2 Grid B data set	56
13. 10-fold cross-validation classification rates for Test 2 Grid B data set.....	57
14. Random sampling misclassification rates for Test 2 Grid B data set	57
15. Terminal node details for Test 2 data set.....	59
16. Misclassification rates for pruned Test 2 data set, 10-fold cross-validation	62
17. Misclassification rates for Test 3 data set, 10-fold cross-validation	63
18. Misclassification rates for Test 4 data set, 10-fold cross-validation	67

19. Terminal node details for Test 4 data set.....	68
20. Misclassification rates for pruned Test 4 data set, 10-fold cross-validation	69
21. Misclassification rates with AT-SST and DP-SST predictor variables.....	71
22. Terminal node details with new AT-SST and DP-SST predictor variable.....	73
23. Misclassification rates for pruned tree with AT-SST and DP-SST variables	74

**FORECASTING ADVECTIVE SEA FOG WITH THE USE OF
CLASSIFICATION AND REGRESSION TREE ANALYSES FOR
KUNSAN AIR BASE**

I. Introduction

Due to the geography of the East Asian continent, the formation of sea fog over Korea is very difficult to forecast. This weather phenomenon occurs year-round, with a maximum frequency in the spring and summer months. The result is significant impacts to the planning and execution of military operations in the region. A tool to predict the onset and duration of sea fog events with a 24-hour lead time would be of immense benefit to military personnel, with positive impacts on flight safety, training, and mission execution. The 8th Operation Support Squadron Weather Flight (8th OSS/OSW) based at Kunsan Air Base, Republic of Korea (Kunsan AB, ROK) requested this product to aid in the successful planning of these events instead of reacting to them as they occur.

1.1 Statement of the Problem

Advection sea fog, usually a spring and summer phenomena, causes dramatic decreases in ceiling and visibilities, with significant operational impacts to Kunsan AB. During each sea fog episode, ceilings and visibilities can fluctuate through several forecast categories over a short period of time. Fog is the most frequent cause of ground visibilities decreasing below three miles (FAA and Dept. of Commerce 1965), and stratus clouds can also lower ceilings below flight minimums. Since fog and low stratus are

near-surface phenomena, they are a hazard to aviation primarily on takeoffs and landings (Venne 1997) at Kunsan AB and can obscure targets at other locations.

In an attempt to provide more accurate forecasting methods for the occurrence of sea fog, it is necessary to understand the mechanisms that control the formation of this weather phenomenon. Advection fog is a type of fog caused by the movement of moist air over a cold surface, and the cooling of that air to below its dew point temperature (Glickman 2000). Sea fog is a common type of advection fog whereby the moist air moves over a body of cooler water. To date, there are no reliable forecast techniques (with 24 hours or more lead time) for advection fog at Kunsan AB, mainly due to the lack of understanding of sea fog under various synoptic conditions in this region (Cho et al. 2000), and a lack of understanding of offshore predictors. An analysis of advection fog formation, and its meteorological and oceanographic environments, could provide useful information to understanding the physical processes of fog development over this area. The capability to provide mission commanders with this planning weather is essential for high combat effectiveness and flight safety. A method for advance advective sea fog forecasting must be devised whereby forecasters can provide commanders with accurate weather intelligence information.

1.2 Scope of Research

The first step of this research was to provide the reader with a complete familiarization of the surrounding geography and its effects on Kunsan AB's climate. An understanding of the large-scale global circulation patterns affecting the region is necessary to understand the synoptic situations which lead to sea fog formation. A thorough literature review of fog formation, types of fogs, physical properties, and a

detailed analysis of sea fog was also necessary before proceeding with the predictive work.

There are many causes of sea fog generation. Some sea fog events are dominated by air advection, others by radiation, and some events have several causes occurring simultaneously. Since all mechanisms of sea fog generation in the sea region west of Kunsan AB are still not clearly understood, there exist certain difficulties in the development of forecast equations and numerical modeling solutions for the prediction of sea fog.

At the current time, statistical analysis of empirical methods is the most logical approach for conducting further research on this subject. Internal relationships (known and unknown) exist between all meteorological and hydrological elements with regards to sea fog. Therefore, it is beneficial to use statistical methods to analyze the multiple weather and hydrological parameters, and to determine empirical relationships which are conducive to advection sea fog impacting Kunsan AB.

By using statistical methods, it may be possible to locate a clear relationship within seemingly irregular meteorological data through statistical analyses; objective laws showing the relationships among various weather and oceanic elements may be found. Within the last 10 years, interest has increased in the use of classification and regression tree (CART) analyses (Lewis 2000) for prediction when standard statistical analyses have failed to find any predictive patterns. CART analysis is a decision forecast tree-building technique, which is unlike traditional statistical analysis techniques. CART is often able to uncover complex interactions between predictor variables which may be difficult to uncover using traditional multivariate techniques.

Lewis (2000) used CART techniques for clinical studies, stating that traditional statistical methods are sometimes poorly suited for multiple comparisons. Lewis states that predictor variables are seldom normally distributed and complex interactions or patterns may exist in the data, making it difficult to develop a reliable clinical decision rule without the assistance of CART. When considering the difficulty in forecasting sea fog for Kunsan AB, and the large number of possible predictor variables, CART is a logical solution to use in this climatological research.

Lewis (2000) described a classification problem as consisting of four main components. The first component is a categorical outcome or dependent variable. This target variable, advection sea fog for this research, is the characteristic to be predicted, based on the predictor variables which are the second component. These predictors are the characteristics which are potentially related to the target variable of interest. For this study, sea surface temperature, air temperature, and dew point depression are some of the predictors considered, which are gathered from surface observations and modeled upper air data. The third component is a learning dataset, which is the dataset the model is built from, while the fourth component of the problem is a test or validation dataset, which is used to validate the model with independent data.

1.3 Research Objectives

The occurrence of sea fog has been analyzed for many years. Multiple studies were conducted at the Naval Postgraduate School for sea fog frequency off the California coastline, but few studies have been conducted for the seas surrounding Korea. Cho et al. (2000), conducted a study based on historical data on sea fog and investigated the relationship between sea fog occurrence and its environmental factors around the Korean

Peninsula. Cho's study determined which surface level predictors had a significant impact on sea fog occurrence, but failed to develop methods for forecasting the events in advance.

This research is unique in that it uses offshore analysis data from the Navy Operational Global Atmospheric Prediction System (NOGAPS) model, not just from the surface but through the 850 mb level, to find predictors relevant to the formation of sea fog that may not have been considered previously. To determine which of these predictors may be of importance, the CART approach is applied to formulate a forecast decision tree.

Upon gathering a reasonable sampling of data, the CART technique is used to determine a reliable method for forecasting advective sea fog with a 24-hour lead time. The overall goal of this research is to find some indicators in the meteorological data analyzed that would suggest a reliable forecast of advection fog at least 24 hours in advance. The results of this research are then translated into an operational forecast decision tool (such as a conditional forecast decision tree) for use by forecasters and mission planners to increase weather intelligence capabilities at Kunsan AB.

The following specific objectives are necessary to achieve the overall goal of this research: perform a geographical and climatological overview of the Kunsan AB area; define fog types and formation processes and how they relate to this region; collect sea surface temperature data, upper air data, and surface observational data for Kunsan AB, as well as upstream locations (both over land and the Yellow Sea); properly format and quality check all data to perform thorough statistical examinations in order to compare the dependent variable (sea fog) with various predictors; use data mining CART analysis

on all sets of data to determine predictive relationships of the predictors; if standard statistical methods fail to find any predictive relationships, develop forecast decision trees to assist in choosing the best predictors for forecasting advection fog, after detecting and verifying all statistical relationships; and finally provide the 8th OSS/OSW with a useful product to forecast advective sea fog for Kunsan AB.

II. Background and Literature Review

2.1 Background

Kunsan AB is located in southwest Korea, about 13 km southwest of the town of Kunsan, a port on the Kum River. The base is bordered on the west and south by the Yellow Sea (Fig. 1). The terrain immediately to the north and east is rugged, consisting of numerous hills reaching heights of 27 to 37 meters. About 55 km to the north is an east-west oriented range, with heights approximately 600 meters above sea level. This range is high enough to have significant effect on air moving over Kunsan from the north. Farther east is the Sobaek Range, which forms a north-south interior divide on the Korean peninsula. These mountains have a maximum elevation of 1,067 meters, but have little effect on the weather at Kunsan.



Figure 1. Map of South Korea (adapted from Microsoft, 2001).

There are four major surface ocean currents off the shores of the Korean peninsula (Fig. 2), with the Yellow Sea Current impacting Kunsan AB the most. The Yellow Sea is a shelf sea with maximum depth of less than 100 meters (Cho et al. 2000). The Yellow Sea Current flows with variable speeds and directions depending on the time of year. It is at its strongest in winter, and is driven south along the coastline by northerly winds. In winter, warm currents parallel the south and southeast coasts, while waters off the west coast are colder because of the direction of flow of the Yellow Sea Current from the north and the shallowness of the Yellow Sea (607th WS, 1998). With the weakening of the northerly winds, the Yellow Sea Current becomes variable in speed and direction by the end of March. By June, the Yellow Sea Current is reversed along the southwest coast, and begins to move northward along the western shores. Finally by July, the Yellow Sea Current develops into a closed cyclonic circulation off the west coast of Korea, which causes an upwelling effect and provides conditions favorable for sea fog formation. It is this sea fog which on occasion advects onto the western coastal areas.

2.2 Fog Formation

Before discussing the processes involved with fog formation, the various classifications of fog involved with this study must be defined. According to Glickman (2000), fog is defined as “water droplets suspended in the atmosphere in the vicinity of the earth’s surface that affect visibility.” As the relative humidity increases gradually towards 100 percent, condensation begins on the nuclei. The available nuclei have water condensing onto them, until they eventually become visible to the naked eye (Ahrens 1994). Once

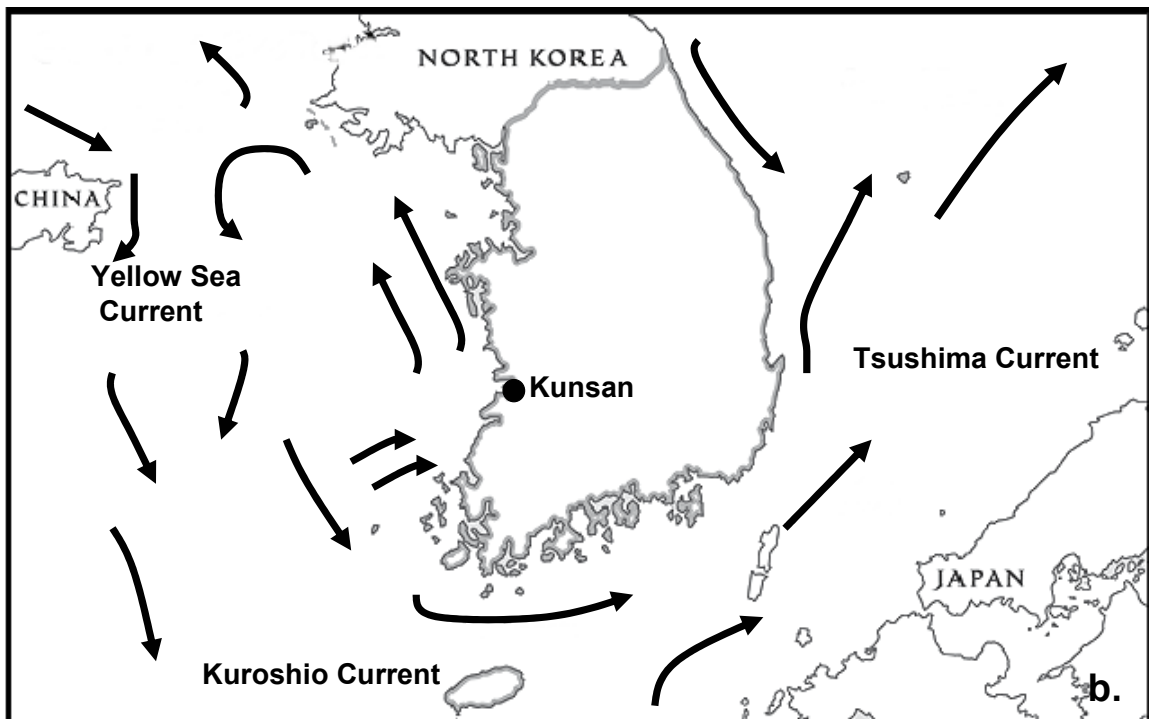
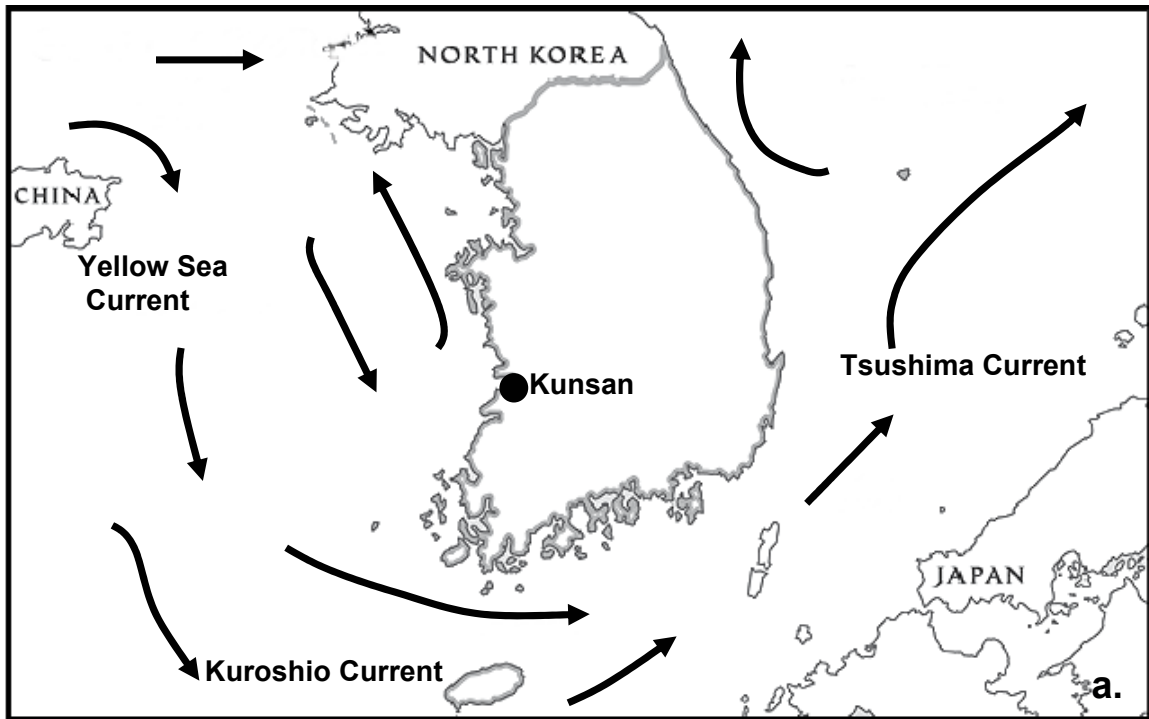


Figure 2. Ocean currents surrounding the Korean Peninsula for (a) Winter (b) Summer (adapted from 607 Weather Squadron, 1998).

the air is filled with millions of tiny floating water droplets, a cloud is visible near the ground which is termed fog.

Advection fog is caused by the movement of moist air over a cold surface, and the consequent cooling of that air to below its dew point temperature. Sea fog is a type of advection fog formed when air that has been lying over a warm surface is transported over a colder water surface, resulting in cooling of the lower layer of air below its dew point temperature. Depending on the wind speed and fetch over water, the interaction between the cooler surface layer and the overlying air may result in low-level stratus as well as fog formation. Advection fogs prevail in locations where two ocean currents with different temperatures flow next to one another (Ahrens 1994). A common location for this is off the coast of Newfoundland in the Atlantic Ocean. The cold southward flowing Labrador Current lies almost parallel to the warm northward moving Gulf Stream. Warm southerly air advecting over the cold current produces fog in that region two out of three days during summer (Ahrens 1994). It is this same type of advective sea fog which is a major forecasting problem at Kunsan AB.

Fog occurs in the lower atmosphere with a height of a few meters, a few tens of meters, or at most hundreds of meters in vertical extent, where the strongest atmospheric influence is the air temperature and water vapor content. Over land, and particularly in the warm season when sea fog is most prevalent, it is difficult to distinguish between radiation fogs and advection fogs (Petterssen 1956). Most land fogs develop as a result of advection followed by radiative cooling. Since the diurnal variation of temperature is large over land, most fogs tend to form in the late evening and dissipate after sunrise. At sea however, the diurnal variation of temperature is small (generally less than 0.5°C).

Nocturnal cooling plays only a negligible part while air advection is the primary cause of fog formation. Instead of dissipating after sunrise like radiation fog, a sea breeze which develops in the late morning can advect the fog inland, where it may persist through the entire day.

Like other general fogs, sea fog forms when the air is saturated and reaches a degree of supersaturation through some atmospheric process (Binhua 1985). There are two ways to increase relative humidity for air saturation, increasing the vapor pressure and lowering the air temperature. Generally speaking, the formation of sea fog is caused by the process of either evaporation or cooling (Binhua 1985). When the two processes occur simultaneously, the effect is more significant.

For the formation of sea fog, an increase in moisture takes place under specific conditions. Increasing moisture is due to the evaporation of water from the sea surface and mixing of air (where moisture decreases in one part of mixing air while increasing in another). Evaporation can only occur when the saturation vapor pressure e_w over the water surface is higher than the vapor pressure e in the air, and the saturated vapor pressure of the air e_a is much lower than e . In simple notation, only when

$$e_w > e > e_a \quad (1)$$

can evaporation increase vapor content in the air, which is favorable for the formation of fog (Binhua 1985). Therefore, evaporation can continue only when the sea surface temperature is higher than the air temperature. In other words, only when a cold air mass moves over a warm water surface can sea fog form through continuous evaporation. Sea fog formation through continuous evaporation is also known as steam fog, and can be

seen over lakes on autumn mornings, when cooler air settles over water still warm from the summer season.

The second process involved with the formation of fog is cooling. Cooling occurs with one or more of the following processes: (1) outgoing long-wave radiation and resultant cooling of the near-surface air; (2) advection of air over a colder surface; (3) adiabatic cooling by orographic, frontal, or turbulent lifting; and (4) evaporative cooling by falling precipitation (Venne 1997). The focus of this study is mostly dealing with cooling caused by advection of air over a colder surface.

The main feature of advection fog is the presence of an advective motion component of air over the sea surface. Both sensible heat exchange and latent heat exchange can occur between the sea surface and the air flowing over it (Binhua 1985). The exchange of sensible heat and latent heat during the formation of sea fog varies with the difference between the air temperature, water temperature, and the relative humidity of the air. Generally speaking, when the air temperature is higher than the water temperature, the sensible heat transfer from air to sea dominates. This is favorable for fog formation by condensation due to cooling of warm air near the surface advecting over the cooler sea surface. Such fog is known as advection cooling fog, with the dew point temperature equal to the surface water temperature. If the surface water temperature is too high, advection cooling fog cannot form. On the other hand, when the air temperature is lower than the water temperature, sea water will be evaporated into the cold air increasing the water vapor content. Such fog is known as advection evaporation fog (or steam fog as previously mentioned). Its formation and dissipation are determined by the range between air temperature and water temperature, as well as saturation vapor

pressure e_w corresponding to the surface water temperature and the actual vapor pressure in the air e . If the temperature range between air and water is large, the evaporation of the water surface will continue to increase water vapor content in the air. In this case, even if the wind is strong, it is possible that the fog will persist (Binhua 1985).

The formation and dissipation of sea fog are related to hydrological factors, among which the local sea current and surface water temperature are the most significant (Binhua 1985). Meteorological factors such as air temperature, humidity, wind, and stability also play key roles. As can be seen from the distribution and variation of sea fog in Figures 3 through 6, the fog favored regions are closely related to the locations of major sea currents. In regions near the shore, such as in the eastern Yellow Sea, fog often occurs where the cold and warm currents meet.

Sea surface temperature, in addition to sea current motion, is one of the most important factors in the occurrence of sea fog. Figure 7 shows the mean sea surface temperature in winter and summer around the southern Korean peninsula. There are a few noticeable cold water regions depicted in the Yellow Sea during the early summer, which are consistent with the high frequency of sea fog occurrences during this time. The cold regions are characterized by shallow water under the strong tidal currents. The shallow water and currents provides enough energy to mix the water column, resulting in a relatively cold sea surface (Cho et al. 2000).

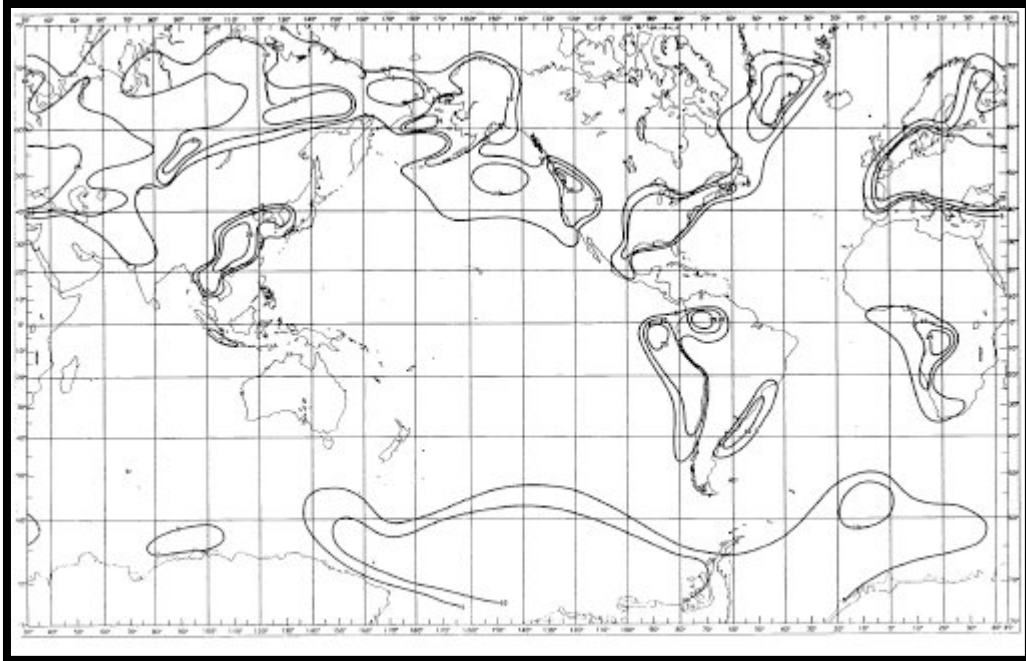


Figure 3. Percentage of fog, January (from Guttman, 1971).

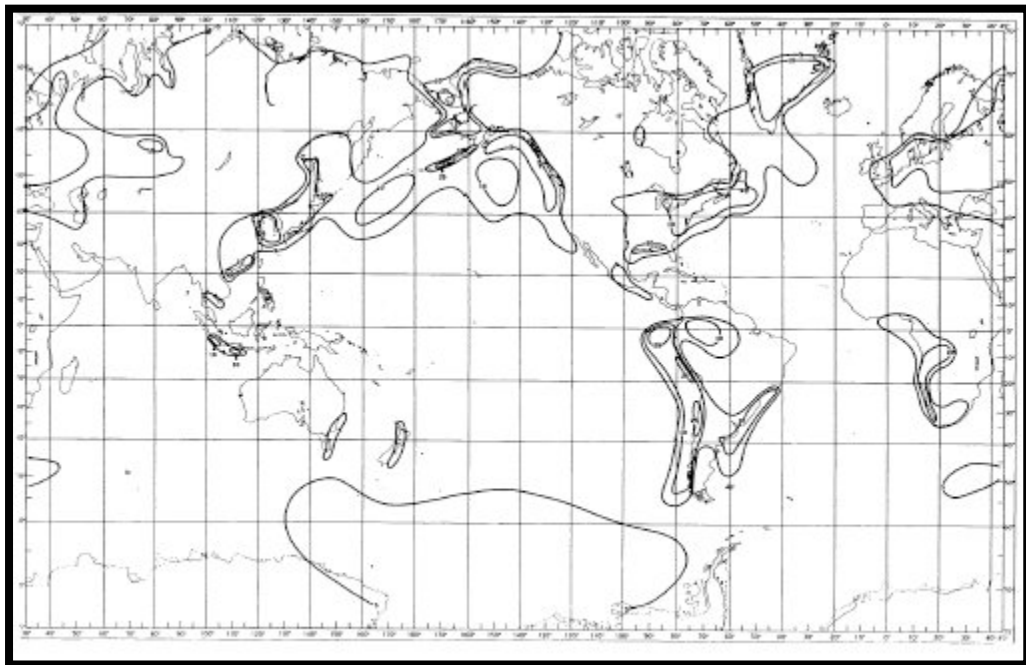


Figure 4. Percentage of fog, April (from Guttman, 1971).

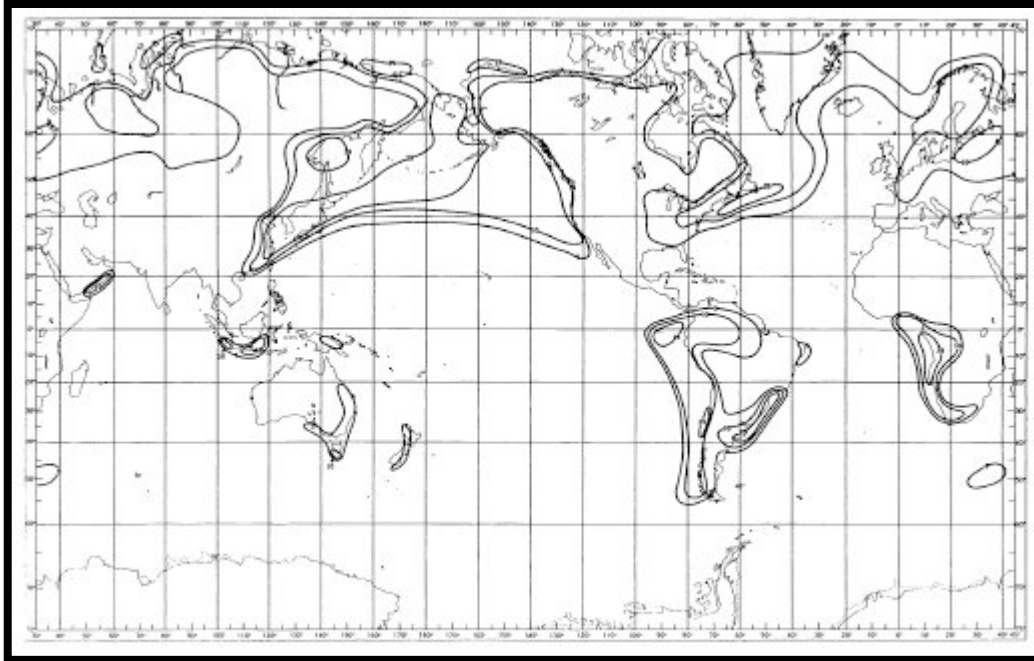


Figure 5. Percentage of fog, July (from Guttman, 1971).

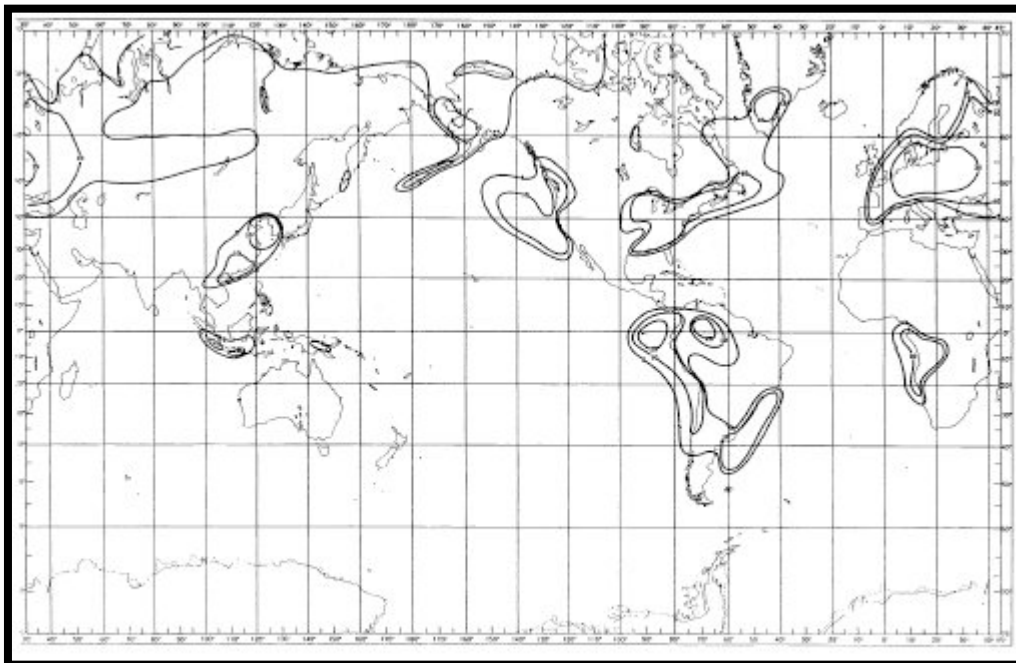


Figure 6. Percentage of fog, October (from Guttman 1971).

A study on monthly mean frequencies of sea fog occurrences was conducted by Cho et al. (2000) for nine coastal and 15 island stations around South Korea. The average rate of occurrence showed that most sea fog occurs during the summer season (Fig. 8), which is similar to the formation of sea fog around the United Kingdom, where sea fog most commonly occurs in spring and early summer (Roach 1995). Cho et al. (2000) also concluded the mean frequency of sea fog occurrence in the Yellow Sea is higher than that of the Sea of Japan. Considering that both the Yellow Sea and Sea of Japan are located at the same latitude, this difference most likely result from the difference in sea surface temperatures.

The formation of sea fog cannot be determined solely from the evaluation of air and sea surface temperatures. The maximum water vapor content at low levels and its variation to surface water temperature must also be considered. As part of their sea fog study, Cho et al. (2000) collected dew point temperature data and made comparisons to sea surface temperatures. It was shown that the highest frequencies of fog (more than 30%) occurred when the difference between the dew point and sea surface temperature was greater than 2° C. The frequency of fog increases with a higher difference between the two values. It is generally accepted that higher dew points relative to the sea surface temperature increases fog probability. If the dew point at the initial forecast time is less than the coldest water temperature, the formation of fog is unlikely (5 WW 1979).

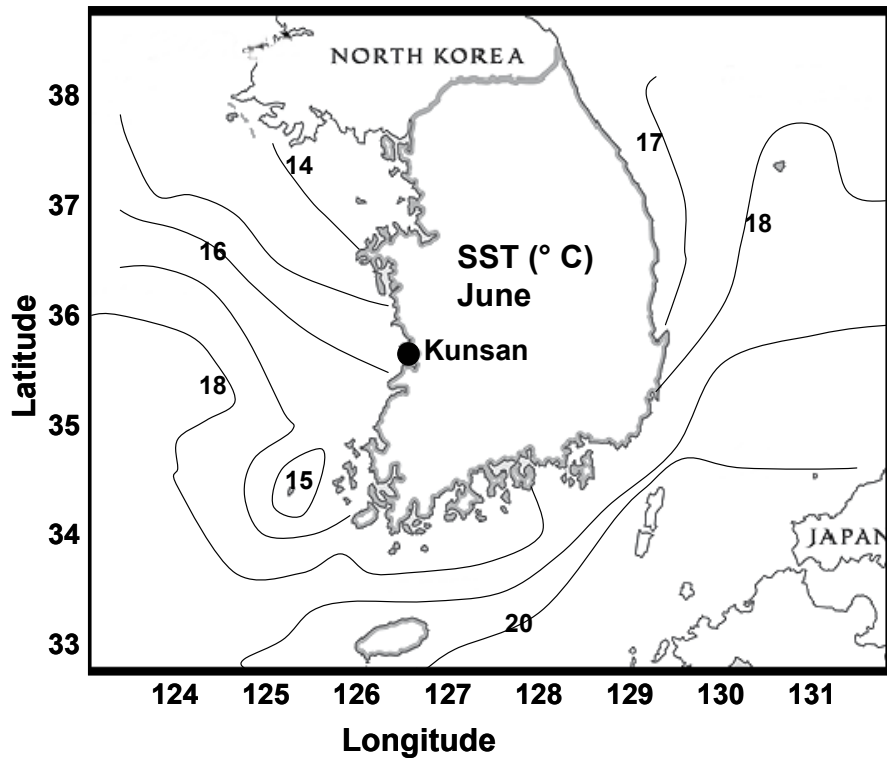
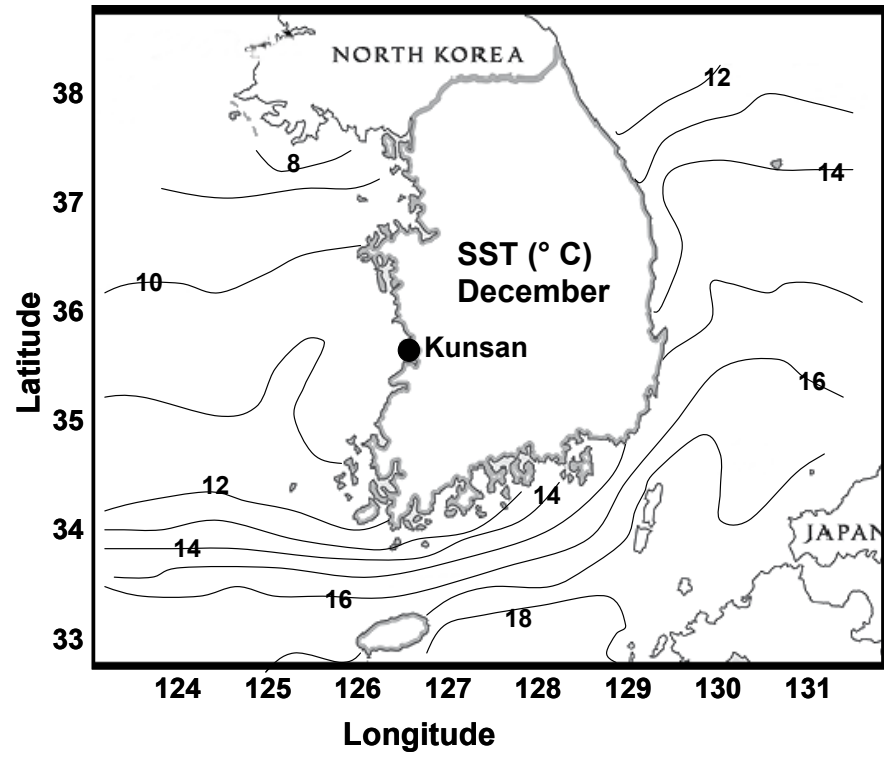


Figure 7. Mean sea surface temperature in (a) Dec and (b) Jun (adapted from Cho et al., 2000).

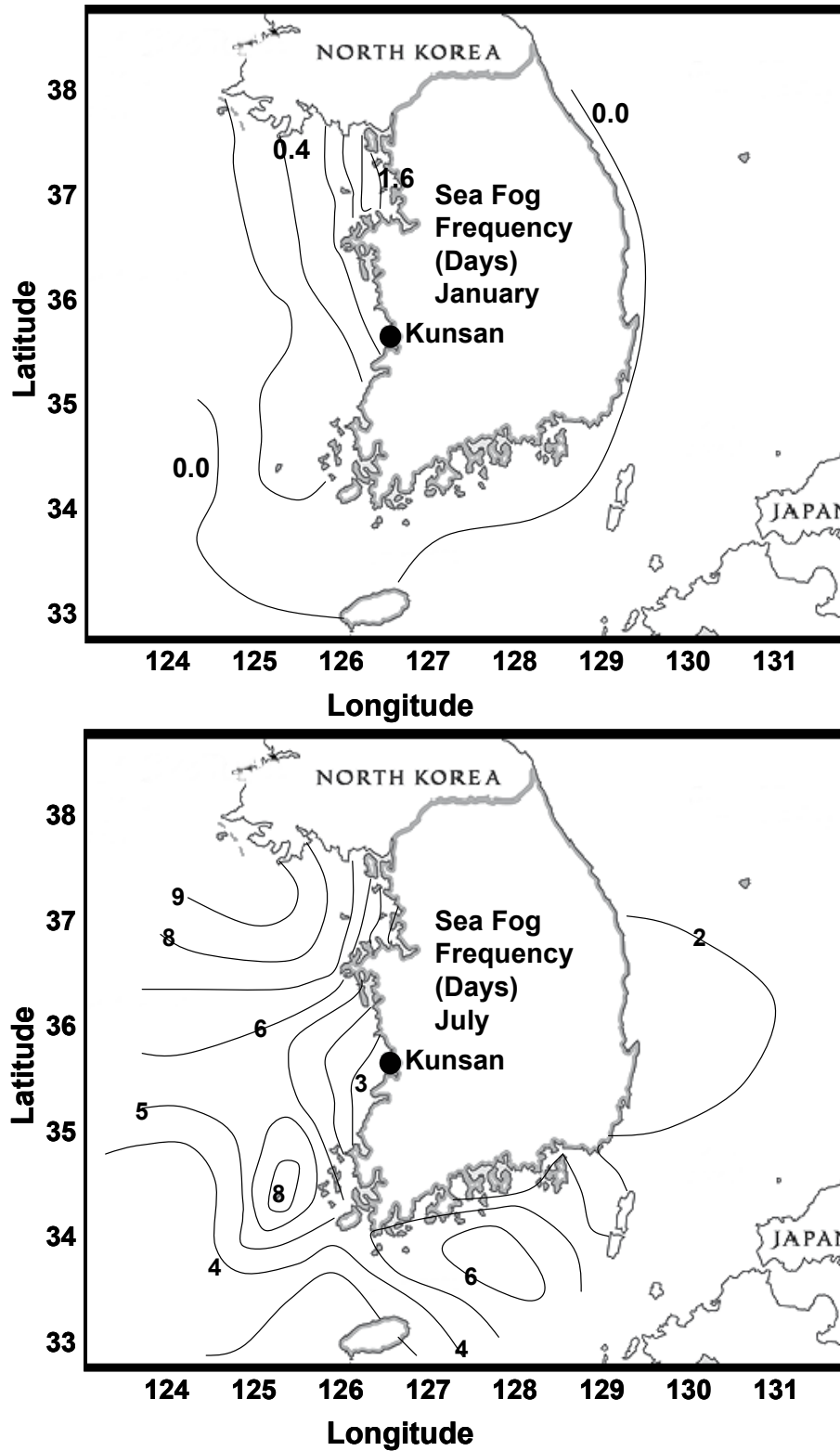


Figure 8. Mean frequency day of sea fog occurrence for (a) Jan and (b) Jul (adapted from Cho et al., 2000).

2.3 Physical Properties of Sea Fog

The density and visibility within sea fog depends on the number concentration and size of fog droplets, as well as liquid water content (Binhua 1985). Neiburger and Wurtele (1949) analyzed observations of visibility and relative humidity off the coast of Los Angeles, California (Fig. 9). It is shown that, on average, the visibility decreases almost uniformly as the relative humidity increases, with the decrease being due to further condensation on the nuclei as air parcels approach saturation (Petterssen 1956).

Under certain conditions, Koschmieder (1924) proposed a formula for the visual range V in a fog as:

$$V = [\log(1/\epsilon)] / \pi r^2 n \quad (2)$$

where V is the visibility in centimeters, ϵ is the ratio of the difference in brightness between the background and the object to the brightness of the background, n is the number of drops per cubic centimeter, and r is the average radius of the drops in μm . In most cases, ϵ is in the range of 0.01 to 0.02. It is seen from Eq. (2) that the visual range is inversely proportional to the total projected area of the drops. Taking ϵ as a constant, Eq. (2) may be written as:

$$V = [C r_m] / w_L \quad (3)$$

where C is a constant, r_m is the radius of the fog drop in μm , and w_L is the liquid water content in g/m^3 . For any given liquid water content, the visual range decreases as the radius of the fog drops decrease. Cloud condensation nuclei are sparse in maritime air, more plentiful in continental air, and abundant in urban air (Orgill 1993). Therefore, in

sea fog, where the drops are relatively large, the visual range would be larger than in a city fog, where the drops are numerous and small.

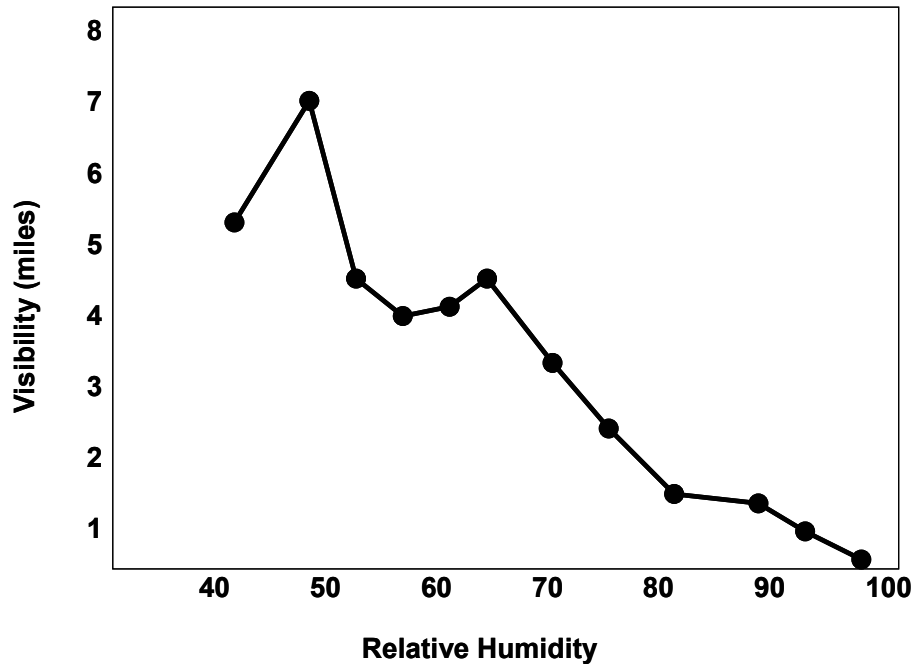


Figure 9. Relation between visibility and relative humidity at Los Angeles Airport (adapted from Neiburger and Wurtele, 1949).

The density of a sea fog expressed in terms of horizontal visibility depends not only on the concentration of fog drops, but also on the liquid water content within the fog. The distribution of liquid water in fog is relatively uniform over large horizontal areas (Wallace and Hobbs 1977). The larger the liquid water content, the greater the density of fog and the lower the visibility. Measurements of liquid water content were taken during the period of June 15-23, 1951, by the Japanese research ship *Yksek Maru* (Binhua 1985). The results showed that the liquid water content in sea fog averaged in a range of 0.1 g/m^3 to 2.0 g/m^3 . The average liquid water content range for land fog is 0.01

g/m^3 to 1.0 g/m^3 . In general, the liquid water content in sea fog tends to be higher than that for land fog.

In a fog region, the concentration of fog drops is defined as the number of fog drops per unit volume. The number and concentration of fog drops decrease if there is an increase in the diameter of the drops given a specific liquid water content (Fig. 10). Fog that forms in dirty city air is often thicker than fog that forms over the ocean. The smaller number of condensation nuclei over the ocean produce fewer, but larger, fog droplets. City air, which has abundant nuclei, will produce smaller droplets, but at a much greater concentration since the nuclei compete for moisture. The concentration of fog drops varies not only with size, but also with temperature variation. When the air temperature is high and evaporation vigorous, large fog drops may become smaller, and small drops may vanish completely due to this evaporation.

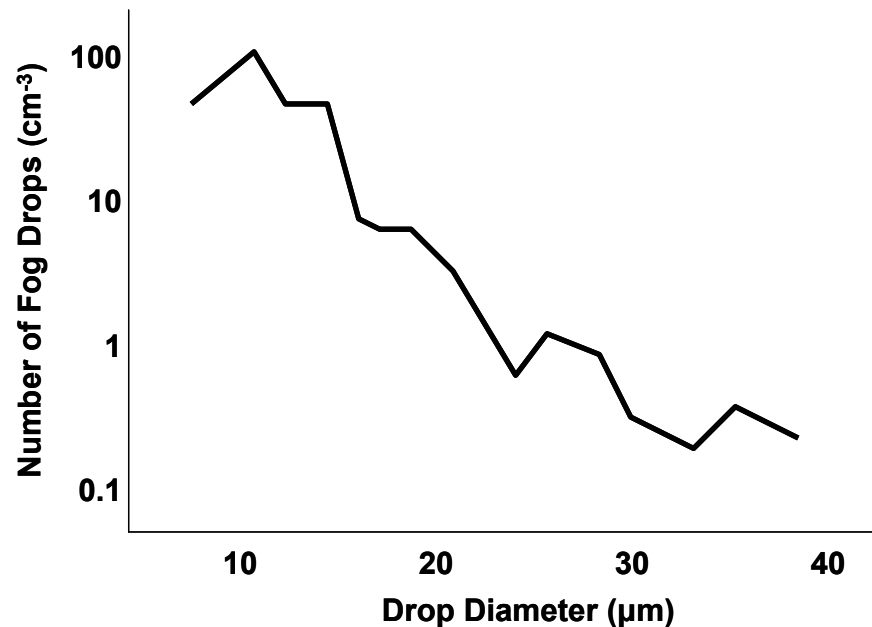


Figure 10. Number of fog drops in relation to their diameter (adapted from Binhua, 1985).

2.4 Dissipation

Fogs have a tendency to dissipate through heating. There is a marked diurnal variation in the frequency of fogs, with a maximum in the early hours and a minimum in the later afternoon. Naturally, a shallow fog will tend to burn off at a higher rate than a deep fog. Most advection fogs are relatively deep, and the deeper ones will withstand diurnal heating (Petterssen 1956). The same is true for fogs which have formed as a result of advection followed by radiation. Since the variation of temperatures over oceans is typically small, sea fogs are not as sensitive to diurnal variations as land fogs.

A light fog without much pollution will have an average liquid water content of 0.03 g/m^3 , while a dense fog may have a value in excess of 0.3 g/m^3 (Petterssen 1956). In order to dissipate a fog, the liquid water needs to be evaporated and the air temperature must be increased so the water vapor resulting from evaporation can be accommodated in the air. When the air temperature is high, only a slight increase is necessary to accommodate the fog water, but a much greater temperature increase is needed with low air temperatures. Fogs that occur at higher temperatures are more sensitive to diurnal variations, while fogs over colder surfaces may persist all day.

One mechanism for dissipating advection fogs near coastlines is the advection over warmer surfaces heated by solar radiation or heated artificially (Orgill 1993). During the dissipation, the fog top moves upward, apparently in response to the increase in turbulence that accompanies the development of an unstable temperature layer over the warmer surface. However, fog movement over a warmer surface is not necessarily sufficient for complete dissipation unless the heat from the surface is distributed throughout the fog layer (Orgill 1993).

This past chapter described the geography of the region and its impacts to the local climate at Kunsan AB. In addition, details on the dynamics of fog formation were reviewed, with specific emphasis on the formation of sea fog. It was determined that hydrological factors and weather conditions within the lower levels of the atmosphere are the most significant for forecasting sea fog phenomena. Using this knowledge, data containing these elements were analyzed for further study.

III. Data Collection and Review

3.1 Data Collection

The period of record (POR) examined in this research is from 1 January 1993 through 31 December 2002 in order to provide a 10 year sample size. Three different sets of data were examined, with multiple variables within each data set. Surface weather observations for Kunsan AB, ROK and sea surface temperature data for the Yellow Sea were obtained from AFCCC databases. Upper air grid data for the Yellow Sea region were obtained from the Navy Operational Global Atmospheric Prediction System (NOGAPS) model, originating from the Fleet Numerical Meteorology and Oceanography Center (FNMOC).

3.1.1 Kunsan AB, ROK Weather Observations. The Kunsan AB weather flight is responsible for providing hourly Aviation Routine Weather Reports (METAR) for the base airfield. The operating hours are seven days a week, 24 hours a day. The observing site is located at 35°55'N, 126°37'E and is at an elevation of 29 feet. The POR for the observations was 10 years, culminating in 101,249 total surface observations.

METAR is a routine scheduled observation as well as the primary observation code used by the United States to satisfy requirements for reporting surface meteorological data (AFMAN 2001). It contains a report of wind speed and direction, visibility, sky condition, present weather, temperature, dew point, and altimeter setting. Normally, points of observation are confined to an area within two statute miles of the observing station, to include phenomena affecting the runway complex, drop zones or landing zones. METAR observations normally reflect the conditions observed at, or seen

from, the usual point of observation within 15 minutes of the time ascribed to the observation (AFMAN 2001).

The observations taken at Kunsan AB for the POR were obtained by a certified weather observer, as opposed to an automated observing system. Limited observer visibility to the northwest makes detection of advection fog difficult for the Kunsan airfield (607th WS 2002). Therefore, while sea fog may have advected into the operating area, documentation may not exist due to observer limitations.

3.1.2 Sea Surface Temperature (SST) Data. SST data were obtained from the Surface Temperature (SFCTMP) model produced at the Air Force Global Weather Central (AFGWC) and collected from the archives at AFCCC. The POR was from 1993 to 2002 and contains surface temperatures from 2816 grid points in the East Asian region. Each grid point contains the surface temperature every three hours, for a total of 8 observations each day. For the purposes of this study, only four of the 2816 grid points were used to correspond with the upper air data obtained from the NOGAPS model.

The SFCTMP model primarily supports the AFGWC Real-Time Nephanalysis (RTNEPH) model at Offutt AFB, Nebraska. The RTNEPH model requires the surface temperature data to make a cloud/no-cloud decision in its infrared thresholding algorithm (Kopp 1995). SFCTMP runs separate analyses for the northern and southern hemispheres, with each hemisphere mapped onto a polar stereographic grid with 1/8th-mesh resolution. The array of gridpoints in each hemisphere is organized into 64 boxes, laid out in an 8 x 8 array (Fig. 11).

Navy SSTs are received once every 12 hours at AFGWC from FNMOC over a whole mesh grid (2.5 x 2.5 degree latitude/longitude). These data are ingested into the

Sea-Surface Processor, which is responsible for skin temperature analyses over all ice-free water points. The data are then remapped over the smaller grid used by SFCTMP.

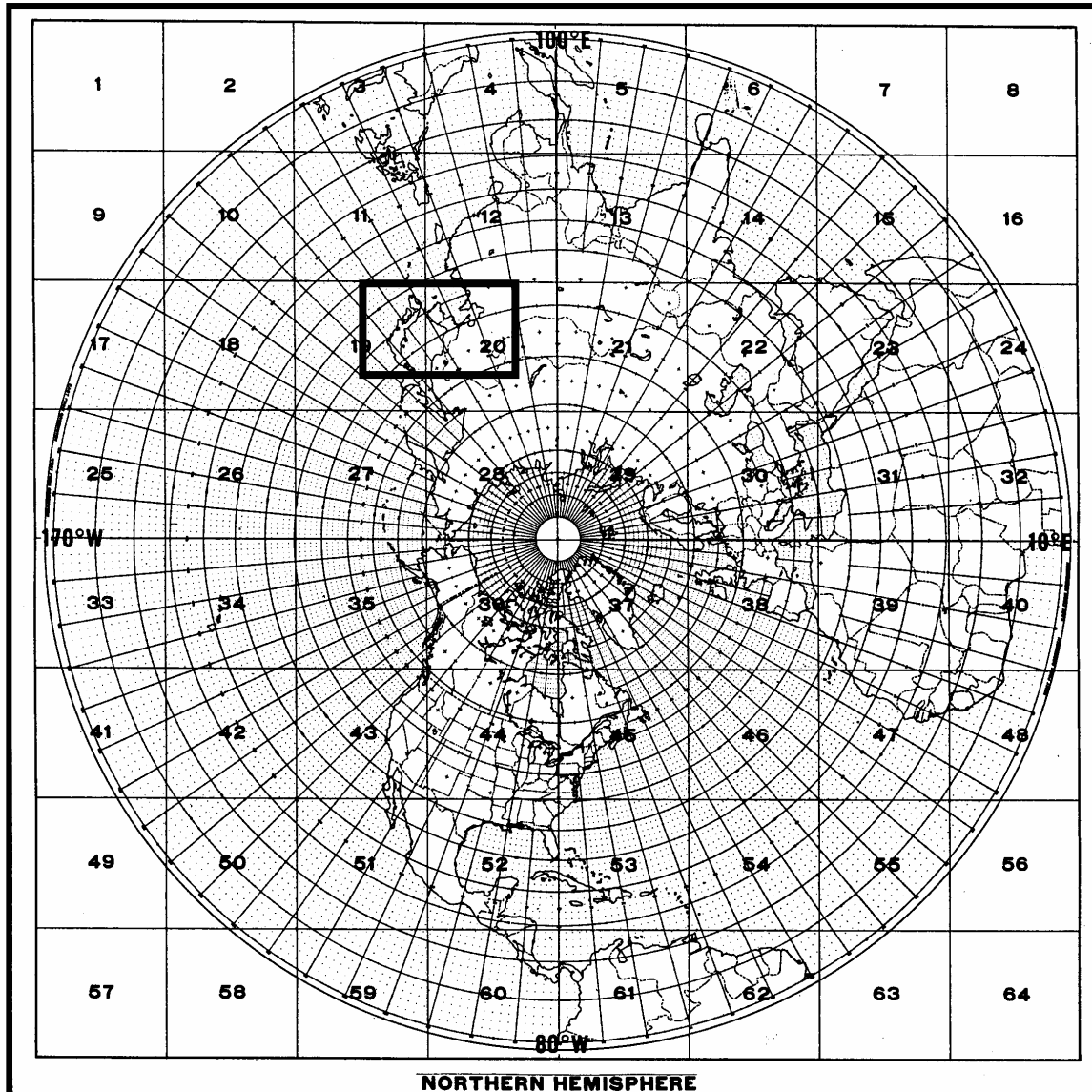


Figure 11. Polar stereographic grid for RTNEPH model (Department of the Air Force, 1986). The highlighted box is the area of interest for this study.

The SSTs then undergo a data quality check each six hour cycle. If any water point contains a temperature colder than 270° K or warmer than 310° K, all SSTs in that

RTNEPH box are carried over from the previous cycle (Kopp 1995). This procedure prevents unrealistic SSTs and avoids an excessively noisy analysis.

3.1.3 Upper Air Data. Upper air data for a POR from 1993 to 2002 was gathered from the NOGAPS model output for the Yellow Sea region. NOGAPS data was obtained on a 2.5 x 2.5 degree latitude and longitude grid, with analysis times of 00Z, 06Z, 12Z, and 18Z daily. Data was collected from a variety of sources; such as land stations, ships, buoys, aircraft, RAOB's, and satellites. The data originates from FNMOC and is sent via the Air Force Weather Agency (AFWA) to AFCCC.

The NOGAPS data for this study are considered to be reliable, considering the techniques used to process the information. Optimum interpolation (OI) is an analysis technique which takes into account three factors: distance between the observation and the grid point, accuracy of the observing instrument, and expected accuracy of the first guess (Department of the Air Force 1991). The first factor, distance between the observation and grid point, is the foundation of nearly every numerical analysis scheme. This factor assigns a weight to the observations around each grid point, with the weight decreasing exponentially with distance. The closer the observation to the grid point, the more weight it receives. Another advantage of OI is its ability to account for differences between various instruments used to record observations. Every instrument is assigned an expected error; the lower the expected error, the more weight the observation from that instrument will have in the analysis. For example, an 850 mb temperature recorded from a Rawinsonde Observation (RAOB) will have more influence in the analysis than an 850 mb temperature

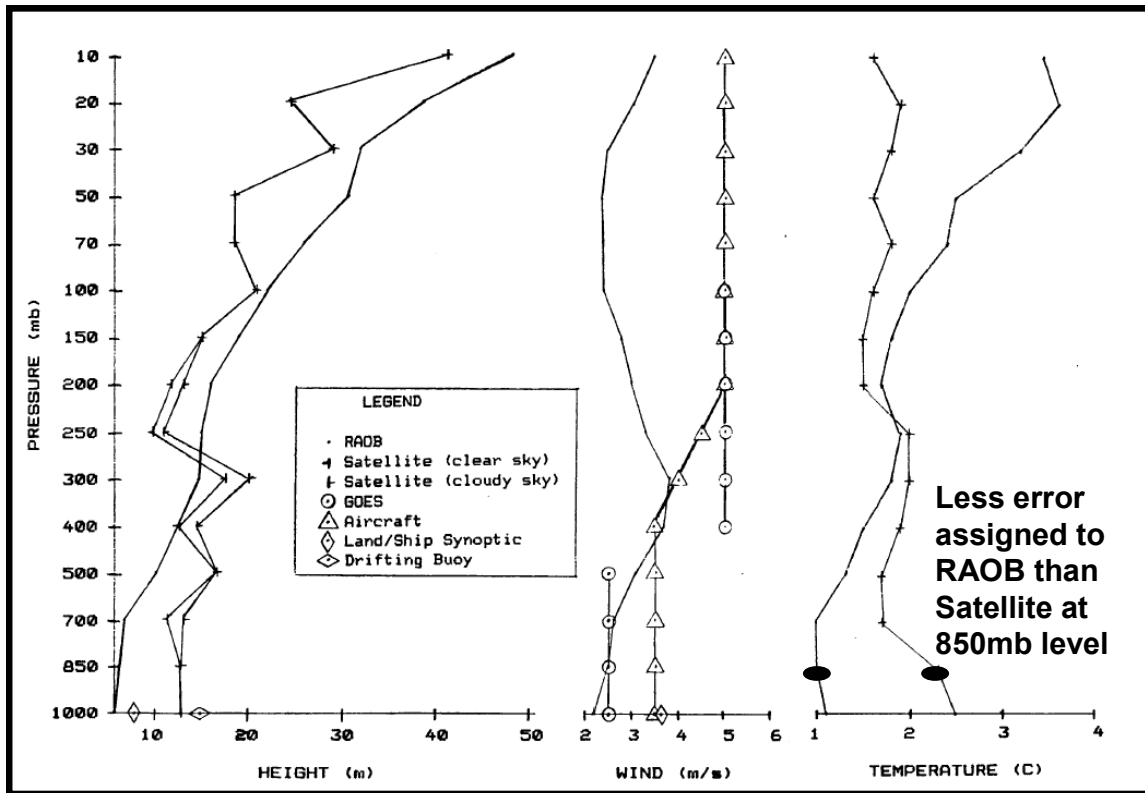


Figure 12. Sample of instrument errors (adapted from Department of the Air Force, 1991).

measured from a satellite (Fig. 12). The reverse would be true for temperature measurements at levels above 250 mb. Finally, OI considers the expected accuracy of the model's first guess by producing error fields, estimating how accurate the analysis is at each grid point. When more observations are available at a particular location, the expected error will be lower, producing a more accurate analysis. For data rich areas such as Europe and Asia, there will be less error than for data sparse areas like the South Pacific. In addition, an inaccurate observation taken in one of the data rich areas will have less impact on the analysis. The techniques used by OI increase the likelihood of accurate analyses, and given the data rich region of this study, the data obtained for this research can be considered reliable.

The data used for this research included temperature, dew point depression, wind direction and wind speed for the surface, 1000 mb, 850 mb, 700 mb, 500 mb, and 300 mb levels. These data include four points covering a square grid west of Kunsan: 122.5E/35N, 125E/35N, 122.5E/37.5N, and 125E/37.5N (Fig. 13). While data were acquired from the surface through 300mb, only the lower atmospheric levels (surface to 850mb) were evaluated as predictors for this study, since sea fog is a lower atmospheric phenomenon.

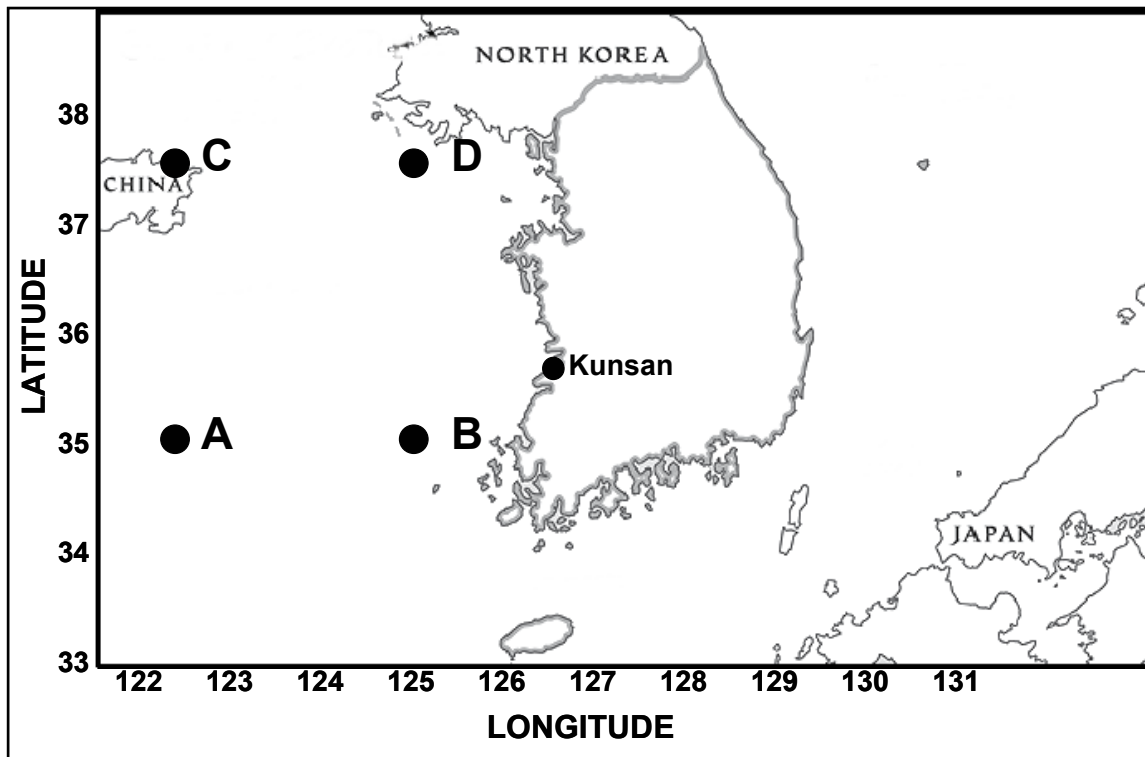


Figure 13. NOGAPS grid points used in this study.

3.2 Data Limitations

A major concern within this research is the relatively short POR of ten years. There are a limited number of sea fog events which impacted Kunsan to analyze within the surface observational data. While sea fog generally moves directly into Kunsan AB

from the southwest, it is possible for it to advect on land further to the west, impacting other operating areas. On these occasions, a lack of observational data may occur due to the limitations of the weather observer's in detecting this phenomenon to the northwest, where sea fog may have advected into the operating area, but not the airfield itself.

A second limitation with the research data is the NOGAPS grid. While the grid box does cover a large portion of the Yellow Sea, there are no data points available for the area immediately to the west of Kunsan. Since past authors have found SST is the most significant predictor to sea fog formation, the lack of SST data directly west of Kunsan may have an impact on determining an exact relationship between the predictor variables and sea fog occurrence at Kunsan.

Finally, some of the data sets had incomplete, erroneous, or missing information. Each of the data sets was carefully reviewed and corrections or deletions were made based on the extent of the errors or absent information. Details on the processes used during quality control are described in the next chapter.

IV. Methodology

This objective of this chapter is to examine the data and focus on producing conditional climatology to aid forecasters in predicting low visibilities associated with advective sea fog. The visibility categories evaluated are derived from the airfield minimum categories used in the Operational Climatic Data Summary (OCDS) from AFCCC (2000). Table 1 is a sample of the frequency for ceilings of 3000 feet and/or visibility less than three statute miles. The table shows the percent frequency of occurrence for each month during different times of the day in Local Standard Time (LST). According to the OCDS, the highest probability of visibility dropping below three miles occurs during June and July, which is consistent with the seasonal frequency of sea fog. Typically for most locations, the highest probability of visibility dropping below category is in the early to mid morning hours when the air temperature approaches the dew point temperature. During June and July at Kunsan AB, the probabilities remain relatively high throughout the day, which is common with a sea fog event.

Table 1. Percent frequency of ceiling/visibility less than 3000 feet/3 statute miles.

LST	Jan	Feb	Mar	Apr	May	Jun	Jul	Aug	Sep	Oct	Nov	Dec	All
0-2	24	24	20	21	23	37	37	19	16	14	21	23	23
3-5	30	28	26	28	30	50	48	29	26	23	25	28	31
6-8	32	32	35	37	36	61	58	39	35	30	29	32	38
9-11	31	28	29	26	27	47	45	25	19	19	24	31	29
12-14	22	20	17	18	17	30	30	14	8	8	14	22	18
15-17	21	19	16	17	15	24	23	13	9	6	13	23	16
18-20	24	20	16	18	17	25	25	14	11	6	12	22	17
21-23	26	21	17	18	20	31	30	15	9	8	14	21	19
ALL	27	24	22	23	23	39	37	21	17	14	19	25	24

4.1 Data Examination

An examination of the data sets was necessary to determine a correlation between the multiple weather parameters and the occurrence of sea fog. Prior to any statistical studies being performed, extensive formatting was required on the data sets to ensure they were usable for regression and data mining tests. This process involved extensive manipulation of the three different sets of data: Kunsan AB surface observations, NOGAPS upper air, and SST.

4.1.1 Surface Observational Database. Upon receiving the Kunsan AB surface observations, quality control (QC) was performed on the data. The review was conducted to determine any typographical errors or locate missing data. There were several cases in 1996 and 1997 when visibility was less than seven statute miles, but present weather condition data was missing. This particular category is important for this research as it is necessary to distinguish between the causes of reduced visibilities, whether it is due to fog, snow, rainshowers, etc. In the event of missing weather information, present weather was manually inputted, as long as the inputted data was supported by meteorological reasoning. For example, if the surface observations prior to or after the observation in question contained reduced visibilities with mist (BR), or BR was mentioned in the remarks section of the observation, then BR was inputted into the data gap. If there were sections of data with excessive missing information, and there were doubts as to the specific weather conditions, the observation was not used for this study.

Upon completion of the QC, classification was completed on the present weather conditions. The goal was to isolate those weather events where visibility was reduced

specifically by BR or fog (FG) from the snow, dust, or rain events. AFMAN 15-111 (2001) defines BR as “hygroscopic water droplets or ice crystals suspended in the atmosphere that reduces visibility to less than 7 miles but equal to or greater than 5/8 mile.” FG is similar to BR, but with visibilities less than 5/8 mile. For the purposes of simplifying the data set for this research, all weather events that are defined as either BR or FG were reclassified as BR. Therefore, if a weather observation has 1/2 mile visibility with present weather FG, it was reclassified as BR.

4.1.2 NOGAPS Upper Air Data. The second set of data contained the atmospheric conditions for each of the four grid points depicted in Figure 13. The data were provided every six hours beginning at 00Z for the ten year POR. QC was performed on the data to located missing information and erroneous values. For any missing data points, the information from the previous six hour model run was used to fill the data gap. If data were missing for two or more consecutive model runs (12 or more hours), the weather information for that time period was not used for the study. In addition, any erroneous data located in the model run (a value of 5000 listed for dew point depression) was replaced with the value from the previous six hour model run. Upon completion of QC, the NOGAPS data were inputted into an Excel workbook, with a specific sheet for each of the four grid points.

For the purposes of using the information in statistical and forecast decision tree programs, it was necessary to merge the surface observations for Kunsan AB and the NOGAPS data into one datasheet. NOGAPS had one set of values for 00Z, 06Z, 12Z, and 18Z, while the surface observations contained a minimum of one entry per hour. In

order to synchronize the surface observations and NOGAPS data on one spreadsheet, the surface observations were reduced from 24 or more a day to four. To accomplish this task, the observations for 00Z, 06Z, 12Z, and 18Z were highlighted for study. The weather information for the previous six hours from each of those highlighted observations was evaluated to determine the average conditions. These average conditions were inputted into the NOGAPS spreadsheet for each of the four time periods of interest. In events of reduced visibilities due to fog, the minimum visibility to occur during the six hour time period was used in the final spreadsheet. The Kunsan AB surface observations were inputted into worksheets for each of the four NOGAPS grid points.

The objective of this study was to produce a tool for providing a 24 hour forecast of sea fog advecting into the Kunsan operating areas. In order to do this, the surface observations were aligned with the NOGAPS data from the previous 24 hours. For example, a 00Z surface observation for 2 January 2000 was inputted next to the 00Z NOGAPS value for 1 January 2000. The purpose was to isolate the fog events, and relate them to the atmospheric conditions which were occurring 24 hours previously, locating parameters that may lead to sea fog formation.

4.1.3 SST Data. The final data set to be examined contained the SST from the SFCTMP model, covering the 10 year POR. The original dataset contained values every three hours with 2816 grid points covering the boxed area depicted in Figure 11. To maintain consistency, the SST data were formatted for inclusion into the main NOGAPS spreadsheet.

The first step was to focus on the SST grid points that were located in close proximity to the four selected NOGAPS grid points. This involved reducing 2816 grid points down to four by comparing the NOGAPS grid in Figure 11 to Figure 13. Next it was necessary to ensure the time periods of the SST coincided with those already selected for the NOGAPS and surface observations. This was a simple procedure involving the removal of the 3Z, 9Z, 15Z, and 21Z from the datasheet, leaving the four selected times of interest. The SST data were then inputted into the main spreadsheet, with the data times and grid points aligned with the NOGAPS data. Any time period with missing SST data was excluded from the study.

4.1.4 Results. The result for the first part of the objective was a thorough dataset to be used for further statistical and data mining study. This dataset contains the observed weather conditions at Kunsan AB aligned with upstream atmospheric and sea surface temperature conditions for the preceding 24 hour time period. There is a separate worksheet for each of the chosen grid points. The next step in the study involves individually testing the target variable against the predictors for each of the four grid points, and determining if a specific upstream location has a greater impact on sea fog advection at Kunsan AB.

4.2 Statistical Analysis

Regression methods have become an integral component of any data analysis concerned with describing the relationship between a target variable and one or more predictor variables. The target variable for this research has only two qualitative outcomes, and is represented by a binary indicator variable taking on values of 0

(visibility greater than 4800 meters) or 1 (visibility less than or equal to 4800 meters). In many fields, the logistic regression model has become the standard method of analysis in a categorical situation (Hosmer and Lemeshow 2000).

4.2.1 Logistic Regression. The difference between logistic regression and the more familiar linear regression is reflected in the use of a binary outcome variable. Once this difference is accounted for, the methods employed in an analysis using logistic regression follow the same general principles used in linear regression.

The accuracy of a model is typically judged by the coefficient of determination R^2 . R^2 can be interpreted as the proportion of the variation of the predictand that is described or accounted for by the regression (Wilks 1995). R^2 values rarely reach unity, and higher values typically indicate better effectiveness. However, this is not the case in logistic regression. Hosmer and Lemeshow (2000) displayed several examples where the value of R^2 was relatively low when compared to R^2 values typically encountered with good linear regression models. Low R^2 values in logistic regression are the norm and present a problem when reporting their values to an audience accustomed to seeing linear regression values. Therefore, R^2 values were not considered with this research. For a more detailed discussion on the specifics of logistic regression, reference Hosmer and Lemeshow (2000).

4.2.2 Logistic Regression Results. It is important to determine if there is a relationship between the target variable and the predictors early in the research. To do

this, initial testing was performed using a statistical software program from the SAS Institute called JMP.

Nominal logistic regression was used when running the tests in JMP. Nominal logistic regression estimates the probability of choosing one of the response levels as a smooth function of the target variable. The fitted probabilities must be between 0 and 1, and must sum to 1 across the response levels for a given target (SAS Institute 2000).

Two values calculated in JMP were considered when reviewing the significance of the predictor variables to the target variable: Chi-Square and Prob>ChiSq. Chi-square is the likelihood-ratio Chi-square test of the hypothesis that the model fits no better than fixed response rates across the whole sample. Typically, the higher the value of Chi-square, the more significant the predictor variable is to the target. Prob>ChiSq is the observed significance probability, often called the p-value, for the Chi-square test. It is the probability of getting, by chance alone, a Chi-square value greater than the one computed. Models are often judged significant if this probability is below 0.05 (SAS Institute 2000).

The data from each of the four grid points in the Yellow Sea were individually inputted into JMP to test for the significance of the predictor variables to the formation of sea fog. The target variable for these tests was Fog < 4800 meters. The predictor variables used in JMP, along with a brief description of each variable, are listed in Table 2. For each grid point, there were thirteen predictor variables considered in the research. The Chi-Square and p-value (Prob>ChiSq) results for the variables from each of the grid points is displayed in Tables 3 through 6.

Table 2. Predictor variables used in JMP.

Predictor	Description
Deg C SST	Sea surface temperature in degree Celsius
SFCTEMP	Surface temperature at grid point
SFCDPD	Surface dew point depression at grid point
SFCDIR	Surface wind direction at grid point
SFCSPD	Surface wind speed at grid point
1000TEMP	1000mb temperature at grid point
1000DPD	1000mb dew point depression at grid point
1000DIR	1000mb wind direction at grid point
1000SPD	1000mb wind speed at grid point
850TEMP	850mb temperature at grid point
850DPD	850mb dew point depression at grid point
850DIR	850mb wind direction at grid point
850SPD	850mb wind speed at grid point

Table 3. JMP results for Grid Point A.

Term	Chi-Square	p-value
Deg C SST	26.24	<0.0001
SFCTEMP	0.05	0.8166
SFCDPD	21.65	<0.0001
SFCDIR	8.20	0.0042
SFCSPD	3.45	0.0631
1000TEMP	4.04	0.0445
1000DPD	8.58	0.0034
1000DIR	8.57	0.0034
1000SPD	36.66	<0.0001
850TEMP	17.63	<0.0001
850DPD	44.66	<0.0001
850DIR	4.33	0.0375
850SPD	27.69	<0.0001

Reviewing the information in Table 3, it can be seen that Deg C SST, 1000SPD, 850SPD, and 850DPD are the most significant predictors for grid point A. The overall Chi-square calculated for this location was 950.2238, with a p-value of <0.0001. This indicates there is a low probability of getting a higher Chi-square by chance alone.

Table 4. JMP results for Grid Point B.

Term	Chi-Square	p-value
Deg C SST	46.42	<0.0001
SFCTEMP	0.05	0.8275
SFCDPD	6.53	0.0106
SFCDIR	9.69	0.0019
SFCSPD	5.94	0.0148
1000TEMP	0.02	0.8915
1000DPD	66.74	<0.0001
1000DIR	6.25	0.0124
1000SPD	26.40	<.0001
850TEMP	2.99	0.0840
850DPD	20.04	<0.0001
850DIR	0.70	0.4018
850SPD	10.55	0.0012

In Table 4, Deg C SST was an important predictor, as well as 1000DPD, 1000SPD, and 850DPD. The overall Chi-square value was 907.9326 with a p-value of <0.0001. For grid point C shown in Table 5, 850DPD had the highest value, followed by SFCDPD and Deg C SST. The overall Chi-square was 1072.539 and the p-value was <0.0001.

Table 5. JMP results for Grid Point C.

Term	Chi-Square	p-value
Deg C SST	48.53	<0.0001
SFCTEMP	0.11	0.7364
SFCDPD	51.43	<0.0001
SFCDIR	23.81	<0.0001
SFCSPD	0.40	0.5273
1000TEMP	8.20	0.0042
1000DPD	2.72	0.0994
1000DIR	0.01	0.9307
1000SPD	19.79	<0.0001
850TEMP	32.12	<0.0001
850DPD	80.03	<0.0001
850DIR	0.49	0.4838
850SPD	30.10	<0.0001

Table 6. JMP results for Grid Point D.

Term	Chi-Square	p-value
Deg C SST	82.71	<0.0001
SFCTEMP	2.52	0.1121
SFCDPD	34.22	<0.0001
SFCDIR	14.86	0.0001
SFCSPD	0.17	0.6792
1000TEMP	8.40	0.0037
1000DPD	40.42	<0.0001
1000DIR	0.06	0.8069
1000SPD	75.41	<0.0001
850TEMP	20.87	<0.0001
850DPD	36.58	<0.0001
850DIR	3.83	0.0503
850SPD	0.48	0.4875

Table 6 shows that Deg C SST is once again an important predictor, along with 1000DPD, 1000SPD and 850 DPD. The Chi-square value was 1146.565 with the p-value once again <0.0001.

One final modeling test, stepwise logistic regression, was run in JMP with the four difference datasets. Stepwise selection of variables is widely used in regression. Employing a stepwise selection procedure can provide a fast and effective means to screen a large number of variables, and to fit a number of logistic regression equations simultaneously. Any stepwise procedure for selection or deletion of variables from a model is based on a statistical algorithm that checks for the “importance” of variables, and either includes or excludes them on the basis of a fixed decision rule. The “importance” of a variable is defined in terms of a measure of the statistical significance of the coefficient for the variable (Hosmer and Lemeshow 2000).

Stepwise logistic regression was performed in JMP for each of the datasets, with the results shown in Table 7. The probability required to be used in the model was set at

0.05. Predictor variables with a p-value value greater than 0.05 will be excluded from the model produced by stepwise regression. The variables are listed in order of importance. In other words, the variables that contribute most to the target variable (formation of sea fog) are shown from most significant to least significant. What these tables suggest is that SST and the upper air predictors have an impact on the formation of sea fog.

Table 7. Results from stepwise logistic regression performed on JMP.

Grid Point A	Grid Point B	Grid Point C	Grid Point D
SFCDPD	1000DPD	SFCDPD	1000DPD
1000SPD	1000SPD	850DPD	1000SPD
850DPD	Deg C SST	1000SPD	850DPD
SFCDIR	850DPD	SFCDIR	SFCDPD
850SPD	850TEMP	850SPD	Deg C SST
850TEMP	SFCSPD	Deg C SST	850TEMP
Deg C SST	850SPD	850TEMP	SFCDIR
1000DPD	SFCDPD	1000TEMP	1000TEMP
1000DIR	SFCDIR		
850DIR	1000DIR		
1000TEMP			

While using JMP has shown that each of the grid points has some predictor variables that relate to the target variable, they do not provide a means for developing a forecast decision tool. It is necessary to establish specific numerical criterion for the predictor variables to aid forecasters in determining whether or not sea fog will advect into the Kunsan AB region. To accomplish this goal, forecast decision trees are produced from a software program designed by Salford Systems called Classification and Regression Tree (CART) analysis, discussed in the next chapter.

V. CART Overview, Method, and Results

5.1 CART Overview

Classification and regression tree (CART) analysis is one of the main techniques employed in data mining (Benz 2003). CART is a single procedure that can be used to analyze either categorical (classification) or continuous (regression) data. A defining feature of CART is that it presents its results in the form of decision trees. The tree structure of the output allows CART to handle massively complex data while producing diagrams that are easy to interpret.

The CART methodology is technically known as binary recursive partitioning (Breiman et al. 1984). The process is binary because the root node is always split into exactly two child nodes and recursive by treating the child nodes as root nodes and repeating the process. In order to split a root node into two child nodes, CART operates by determining a set of questions with “yes” or “no” answers that permit accurate prediction or classification of cases. For example, the question may be:

Is **TEMP** $\leq 7^{\circ}\text{C}$?

For each case the question is used to split the node by sending the “yes” answers to the left child node and the “no” answers to the right.

Once a best split is found, CART repeats the search process for each child node, continuing recursively until further splitting is impossible or stopped. Splitting is impossible if only one case remains in a particular node, or if all the cases in that node have the same predictor variables. CART also allows splitting to be stopped if the node

has too few cases, with the default lower limit set at ten cases for this research. The total number of splits is determined by multiplying the total number of predictors by the amount of records in the data set. For example, if there are ten predictors and 1000 records, then there will be 10,000 different splits considered in formulating the optimal tree.

Once the maximal tree is grown, CART determines the best tree by testing for error rates or costs. With sufficient data, the simplest method is to divide the sample into learning and test sub-samples. The learning sample is used to grow an overly large tree, while the test sample is used to estimate the rate at which cases are misclassified. The misclassification error rate is calculated for the largest tree and every sub-tree. The best sub-tree is the one with the lowest or near-lowest cost.

5.1.1 Tree Splitting Methods. There are six different splitting functions available in the classification analysis: Gini, Symmetric Gini, Entropy, Class Probability, Twoing, and Ordered Twoing. The best known rules for binary recursive partitioning are Gini and Twoing, which were the two methods employed for this research. Because each rule represents a different philosophy as to the purpose of the decision tree, each may grow a different style of tree.

The Gini rule looks for the largest class in the database, and strives to isolate it from all other classes. For example, with two Classes, 0 and 1, the Gini rule would immediately attempt to pull all the Class 0 records into one node. In theory, a perfect split would leave two pure child nodes of Class 0 and Class 1. A pure decision tree is attainable only in very rare circumstances; in most real-world applications, database

fields that clearly partition classes are not available. Gini will attempt to come as close to this ideal as possible by focusing on one class at a time. It will always favor working on the largest class in the node. Gini performance is frequently so good that it is the default rule in CART.

The Gini split searches for the best separation that produces a high amount of purity (homogeneity or lack of variety) in the node (Benz 2003). The Gini impurity criterion for the dataset t is given by:

$$i(t) = 1 - S \quad (4)$$

where S is the sum of the squared probabilities $p(j / t)$ from each class. For a two class example node with 50 observations, 40 in Class 0 and 10 in Class 1, the impurity calculation would be written as follows:

$$i(t) = 1 - [(40/50)^2 + (10/50)^2] = 0.32 \quad (5)$$

Therefore, the impurity calculated for the above sample node would be 32 percent.

An alternative splitting criterion in CART is the Twoing function, which operates by separating the classes into two groups that add up to 50 percent of the data. The concept is based on class separation rather than node heterogeneity. The objective is to make the likelihood that a given class j case goes to the left as different as possible from the probability that it goes to the right (Benz 2003). The function sums the absolute value of the probability differences over all j classes, with the formula given as:

$$\frac{p_L p_R}{4} \left[\sum_j |p(j | t_L) - p(j | t_R)| \right]^2 \quad (6)$$

where $p(j | t_L)$ and $p(j | t_R)$ are the probabilities of an object being distributed into Class j given left and right terminal nodes respectively (Breiman et al. 1984).

The rationale for the Twoing function is quite different from that of Gini. For a multi-class problem, Twoing operates by dividing the classes into two groups, gathering similar classes together, and attempting to separate the two groups in the descendant nodes. It thus treats every multi-class split as if it were a two-class problem.

For the two-class problem, such as this research, the Gini and Twoing criteria are mathematically equivalent. The tree structures are the same, as is the overall predictive tree accuracies. If there are multiple classes and the performances of the criteria differ substantially, Gini tends to yield the better splits and therefore is the default in CART (Salford Systems 2001).

5.1.2 Priors. To further assist the algorithm in making the best splits, the researcher must inform CART of the nature of the categorical class distribution (Benz 2003). When data are gathered from samples stratified on the target variable, the class proportions observed in the data may be far from the population proportions (Salford Systems 2001). The method used for adjusting the analysis for this circumstance is known as *Priors*.

Priors equal is the default setting used in CART, and treats the classes in the sample as if they were uniformly distributed in the population regardless of the observed sample proportions. With the *priors equal* setting, CART pays no attention to how rare a class is in the dataset. Instead, CART looks at whether a given node is more or less rich in that class as compared to the root node. This default setting frequently gives the most satisfactory results because each class is treated as equally important for classification accuracy (Salford Systems 2002). Another setting is *priors data*, which means the

probabilities of each class occurring match the total sample frequency (Benz 2003). The other options provided in CART are *priors mix*, *learn*, *test*, and *specify*, which are not evaluated for this research.

5.1.3 Pruning Trees. CART will continue to grow trees until it is not possible to grow them any further, either because it is no longer able to split or until the maximum node size is reached. Breimen et al. (1984) recommends letting the splits continue until pure classification is achieved. This pure result, containing thousands of nodes and thereby unrealistic to use in a climatological study, would then be pruned upwards providing results that have a more meaningful interpretation.

5.1.4 Testing. The best tree is determined by estimating its expected cost. Generally, using a separate test data set provides the most accurate assessment of the true error rate of a sequence of trees, providing there are a sufficient number of test cases. There are five testing options available in CART, two of which were used in this research: cross validation and fraction of cases selected at random for testing.

5.1.4.1 Cross Validation. 10-fold cross validation is typically used when there is insufficient data available for a test sample, typically less than 3,000 observations. However, cross validation can also be useful when analyzing a dataset with a rare target class, such as sea fog which is the target in this research. In this instance, the total number of observations is well above 3,000, but the class of interest has only a small proportion of records.

Using cross validation, CART grows a maximal tree on the entire learning sample. This is the tree that will be pruned back. CART then proceeds by dividing the learning sample into 10 roughly equal parts, each containing a similar distribution of the target variable. CART takes the first nine parts of the data, constructs the largest possible tree, and uses the remaining 1/10 of the data to obtain initial estimates of the error rate of selected sub-trees. The same process is repeated on another 9/10 of the data while using a different 1/10 part as the test sample. The process continues until each part of the data has been held in reserve one time as a test sample. The results of the 10 mini-samples are combined to form error rates for trees of each possible size (Salford Systems 2001).

5.1.4.2 Fraction of cases selected at random for testing. This option allows CART to automatically separate a specified percentage of cases of data for testing purposes. This method is only recommended when there are a minimum of 3,000 observations available within the data set. The data selected for testing is random, and there is no way to find out which records were used for the learning data set and the test data set.

5.1.5 Class Assignment. It is important to understand the methods used in CART when assessing the class assignment for each particular node; the percent error misclassification stems directly from class assignment. The probability of a record going into the left child node with Class n is computed with Bayes' Theorem:

$$p(n_0 | L) = \frac{p(L | n_0) p(n_0)}{p(L | n_0) p(n_0) + p(L | n_1) p(n_1) + p(L | n_2) p(n_2)}. \quad (7)$$

where n_x is Class 0,1 or 2. When using priors equal, the probability of Class n is the number of cases in the left node over the total number of cases for that class. Consider an

example with two classes calculated with priors equal. The distribution of each class for the root and child nodes is shown as:

	<u>Root</u>	<u>Left</u>	<u>Right</u>
Class 0	10560	6633	3927
Class 1	2026	1714	312

Using Bayes' Theorem, the within node probabilities are calculated as:

	<u>Left</u>	<u>Right</u>
Class 0	0.426	0.707
Class 1	0.574	0.293

where the class assignment for the left node is 1 and 0 for the right node. All the records not of the assigned class contained in the node are misclassified. The percent error misclassification is the sum of the misclassifications per class of each terminal node of the entire tree.

5.2 Cart Methodology and Results

Prior to the construction of the classification trees, the data were properly formatted with the fog target variable reclassified from continuous to categorical values (for details on formatting, see section 4.1). Table 8 shows a list of all the variables considered for CART testing. The overall goal when testing the data is to find a decision tree which yields 30 percent or less misclassification error rates for the Class 1 fog variable.

Before running the primary tests on CART, it was determined to use only grid point B for producing the forecast decision trees. Although some correlation was found between the target variable and predictor variables for each of the four locations, grid

point B maintained some of the strongest correlations for each of the predictor variables. It was decided to focus on the data from this particular point for developing forecast decision trees.

5.2.1 Initial Classification Testing. The initial dataset used for this research was for grid point B (see Fig. 13), which contained a total of 12,586 records. Given this amount of data, there were over 100,000 splits possible when running classification trees in CART. The initial Class 1 target variable established for this research included all events with visibility less than or equal to 4800 meters and present weather coded as BR (fog). This eliminated those weather events where visibility was reduced due to rain, snow, or other weather phenomena. One significant limitation to this categorization is it does not distinguish advection fog events from radiation fog events, which could have a severe impact on the final outcome.

To begin the testing, the data set was run using the first 13 predictor variables from Table 8 against the target variable $\text{Fog} \leq 4800$. The number of observations for fog events accounts for approximately 16 percent of the data; therefore, *priors equal* was used for all the classification trees so each class would be treated as equally important.

Testing was performed twice, once with 10-fold cross-validation and another with random sampling (20 percent of the data set aside for testing). The results from the Gini and Twoing methods were compared during the initial test to confirm mathematical equivalency. It is noted in Table 9 that there is not a difference in the relative cost (percent error left unexplained by the decision tree) between Gini and Twoing, due to the nature of this research as a two class problem. Therefore, Gini will be the primary

method used for the classification trees. The percent misclassification and percent prediction success rates are documented in Tables 10 and 11, with the classification trees produced through 10-fold cross-validation and random sampling depicted in Figures 14 and 15.

Table 8. List of predictor variables used for CART.

Predictor	Description
Deg C SST	Sea surface temperature in degree Celsius
SFCTEMP	Surface temperature at grid point
SFCDPD	Surface dew point depression at grid point
SFCDIR	Surface wind direction at grid point
SFCSPD	Surface wind speed at grid point
1000TEMP	1000mb temperature at grid point
1000DPD	1000mb dew point depression at grid point
1000DIR	1000mb wind direction at grid point
1000SPD	1000mb wind speed at grid point
850TEMP	850mb temperature at grid point
850DPD	850mb dew point depression at grid point
850DIR	850mb wind direction at grid point
850SPD	850mb wind speed at grid point
DP-SST	Difference between dew point and SST
AT-SST	Difference between air temperature at SST
RKJKDIR	Wind direction at Kunsan AB
RKJKSPD	Wind speed at Kunsan AB

Table 9. Initial relative cost comparison for Grid B data set.

	Gini	Twoing
Cross Validation	0.690	0.690
Random Testing	0.712	0.712

Table 10. 10-fold cross-validation misclassification rates for Grid B data set.

Class	Total Cases	Learn Data Error	Test Data Error	Learn Data Success	Test Data Success
0	10560	34.53%	34.37%	65.5%	65.6%
1	2026	31.15%	34.60%	68.9%	65.4%

Table 11. Random sampling misclassification rates for Grid B data set.

Class	Total Cases	Learn Data Error	Test Data Error	Learn Data Success	Test Data Success
0	8414	40.56%	41.89%	59.4%	58.1%
1	1613	25.67%	29.30%	74.3%	70.7%

The percent error misclassification rate for 10-fold cross-validation of Class 1, the fog target variable, is 31.15% and 34.60% for learn and test data respectively. The misclassification rates of Class 1 for random sampling testing were lower at 25.67% and 29.30%. As indicated from Table 9, the overall relative costs associated with random sampling for this data set is higher, indicating a higher error rate covering all the data. It is noted that Class 0 events have better results with 10-fold cross validation and Class 1 events have better results with random sampling. With the smaller percentage error rates associated with Class 1 individually, it would seem the random sampling is an acceptable test to use with this data set since classifying Class 1 events is the primary goal.

Figure 14 displays the classification tree produced from 10-fold cross-validation. It is important to recognize that four of the root nodes had the same splitting criteria and ranked in the same order of importance that was determined from the stepwise regression performed on JMP (Table 7): 1000DPD, 1000SPD, Deg C SST and 850DPD. Similar results from two statistical programs give confidence that these particular predictor variables are of importance to the forecasting of fog events.

Figure 15 is the decision tree for the same data set using the random sampling method. From Table 9, the overall relative cost was higher for this test, but the fog event misclassification was lower. One thing to observe from the decision tree is the similarity

in split criteria for nodes 1 through 6 for each of the methods. The predictor variables are the same for those particular nodes, although the specific split criteria (ex. $1000DPD \leq 6.250$ versus $1000DPD \leq 5.050$) differ somewhat. In random sampling, a slightly higher percentage of Class 1 fog events are split to the right of the tree from node 1 to node 8, resulting in further splitting on that side of tree that did not occur with 10-fold cross-validation. This percentage is still fairly minor when compared to the number of events on the left side of the decision tree, which is where the primary focus will be.

Upon studying the split criteria from the first two trees, a potential problem with the arrangement of the wind data was observed for node 5 and terminal nodes 2 and 3. The split criterion for these terminal nodes was 850DIR, the 850 mb wind direction. The winds were split at $850DIR \leq 293.500^\circ$ and $850DIR \leq 289.500^\circ$ for Figure 14 and Figure 15 consecutively. The wind direction is arranged around a 360° circle as depicted in Figure 16. As can be seen from the shaded area of the graph, any winds that would be less than 293.5° could fall within quadrants I, II, III or part of IV. Since this covers such a large spectrum of values, the splitting of node 5 would only be of minimal use. The method employed to overcome this dilemma was to review the data, and determine if there were any sections of wind that could be deleted from the data set.

5.2.2 Testing with the removal of 0° through 135° NOGAPS winds. By reviewing the complete data set, it was determined that observations with winds from the northeast at grid point B could be deleted from the data set, with the assumption those winds would advect sea fog away from the Kunsan operating area. Observations with SFCDIR, 1000DIR, and 850DIR NOGAPS values between 0° and 135° accounted for 35 percent of

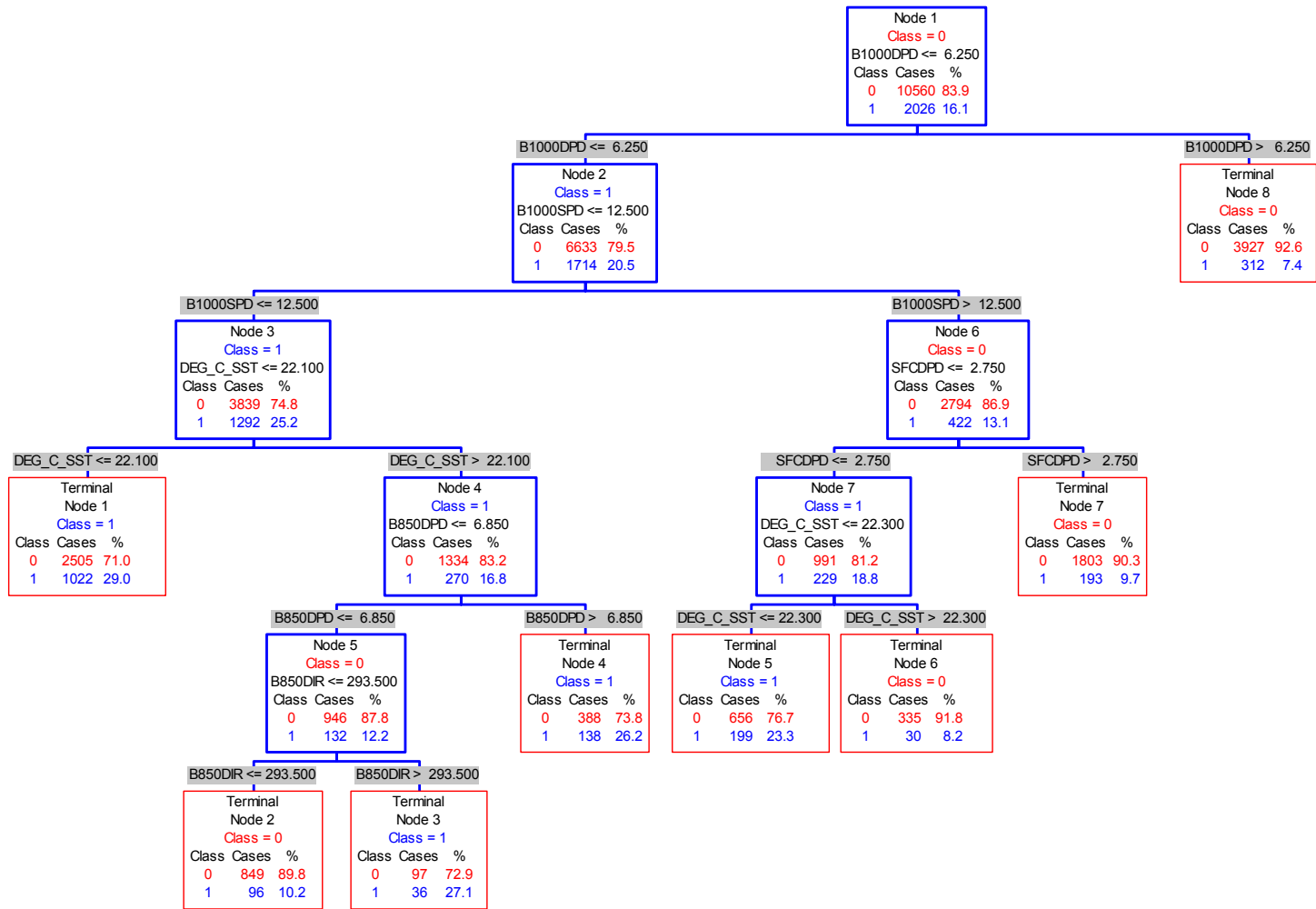


Figure 14. Forecast decision tree using Gini, 10-fold cross-validation. In node 1, the second line contains the class designation; the third line is the conditional statement. A yes response follows the next level into the left node, while a no response follows down a level to the right node.

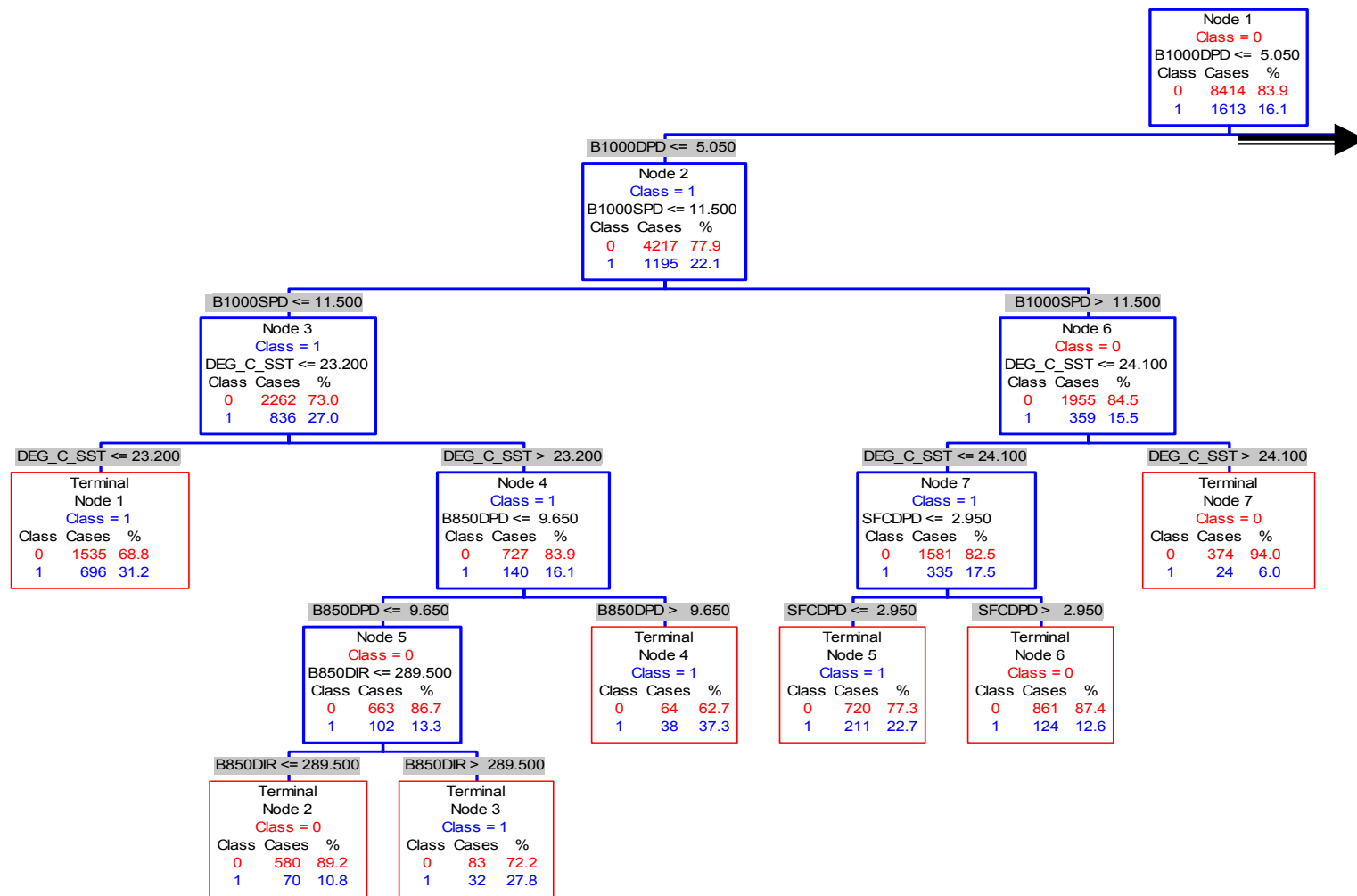


Figure 15. Forecast decision tree using Gini, random sampling. With random sampling, only 80% of the observations are used to produce the decision tree, as compared to 100% of the observations from 10-fold cross-validation.

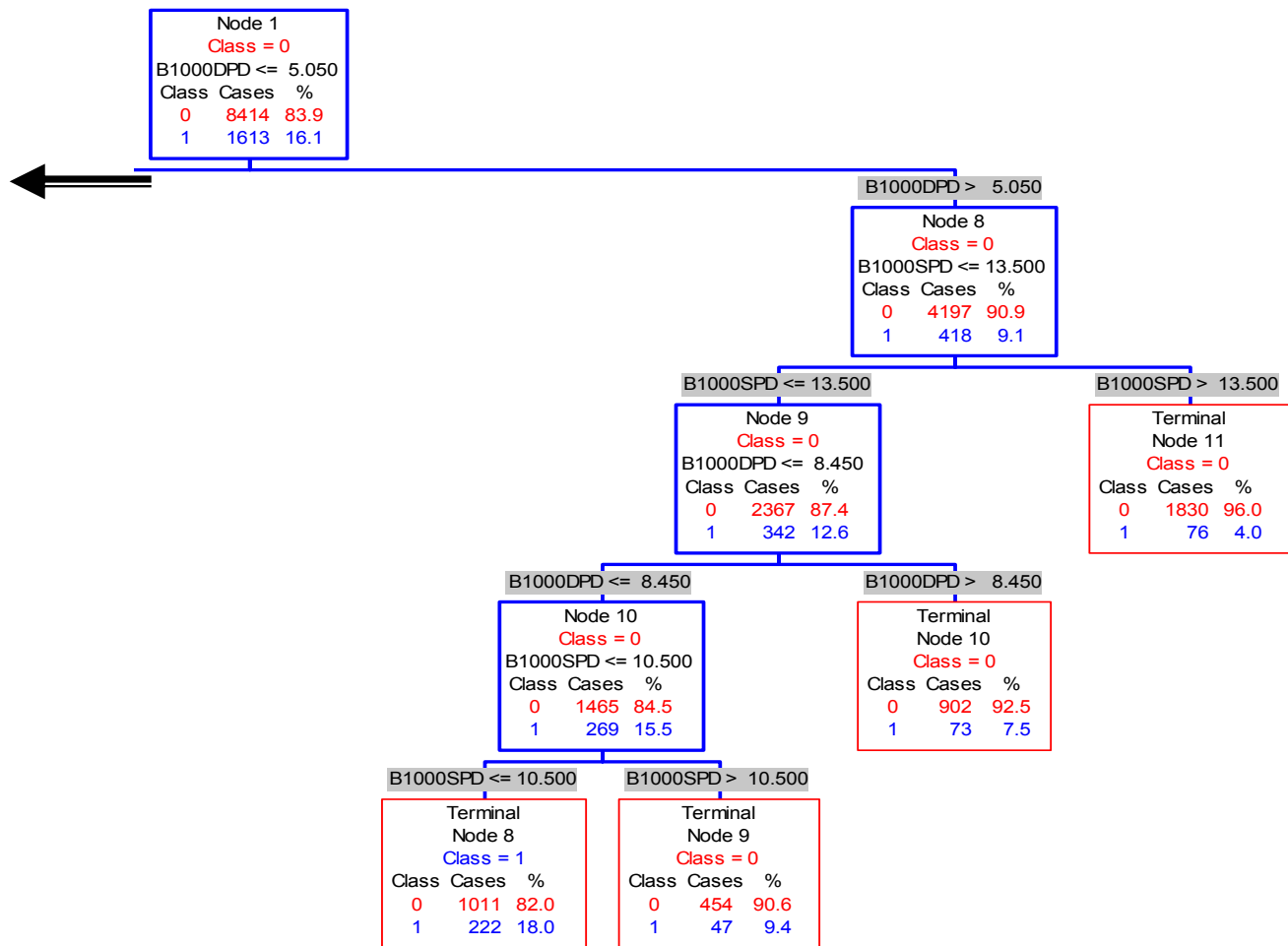


Figure 15. (Continued).

the total data set, and 36 percent of all fog events (including radiation fog). Those observations were deleted from the initial data set, renamed as “Test 2”, and another set of tests were conducted with 10-fold cross-validation and random sampling, with the results displayed in Tables 12 through 14.

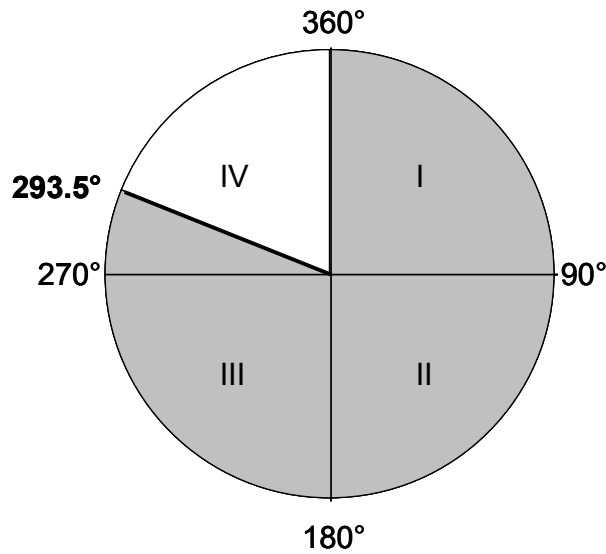


Figure 16. Wind circle diagram. The wind data is given in degrees, with the numerical value giving the direction the wind is moving *from*. The top of the graph is north, and begins with 0°, moving about the circle in a clockwise direction. Quadrant I is all winds from the northeasterly direction, quadrant II southeasterly, quadrant III southwesterly, and quadrant IV northwesterly, completing the circle at 360° north.

Table 12. Relative cost comparison for Test 2 Grid B data set.

	Gini	Twoing
Cross Validation	0.645	0.645
Random Testing	0.691	0.691

Table 13. 10-fold cross-validation misclassification rates for Test 2 Grid B data set.

Class	Total Cases	Learn Data Error	Test Data Error	Learn Data Success	TestData Success
0	6877	35.87%	35.61%	64.1%	64.4%
1	1300	20.46%	28.85%	79.5%	71.2%

Table 14. Random sampling misclassification rates for Test 2 Grid B data set.

Class	Total Cases	Learn Data Error	Test Data Error	Learn Data Success	Test Data Success
0	5465	30.69%	31.94%	69.3%	68.1%
1	1039	21.37%	37.16%	78.6%	62.8%

As indicated by Table 12, the Gini and Twoing methods once again produced identical relative cost comparisons; therefore, the Gini method was used for all further testing. From Table 13, the percent misclassification rate for 10-fold cross-validation of Class 1 events is 20.46% for learn data and 28.85% for test data. This is an improvement from the initial forecast decision tree in Table 10 of 34% for learn data and 17% for the test data from the initial testing. From the random sampling testing results shown in Table 14, the percent misclassification for learn and test data was 21.37% and 37.16%, with an improvement of 16% for the learn data set. However, there was an 8% increase in the number of Class 1 events misclassified when comparing the test data against the learn data set when building the tree. This indicates the removal of the winds increased the overall quality of the forecast decision tree, but for this particular data set, 10-fold cross-validation provides better results than random sampling. 10-fold cross validation is the preferred testing method due to the reduction in Class 1 cases after the removal of wind data.

As discussed previously, 10-fold cross-validation is the preferred method when there are a limited amount of observations available in the data set. With the removal of 35 percent of the total data set, there are now only 1300 Class 1 events (Table 13) to test. In random sampling, when 20% of the data set is removed for independent testing, only 1039 Class 1 cases (Table 14) were available. Since the misclassification rates continue to increase with fewer observations, only 10-fold cross-validation will be used for any further forecast decision trees.

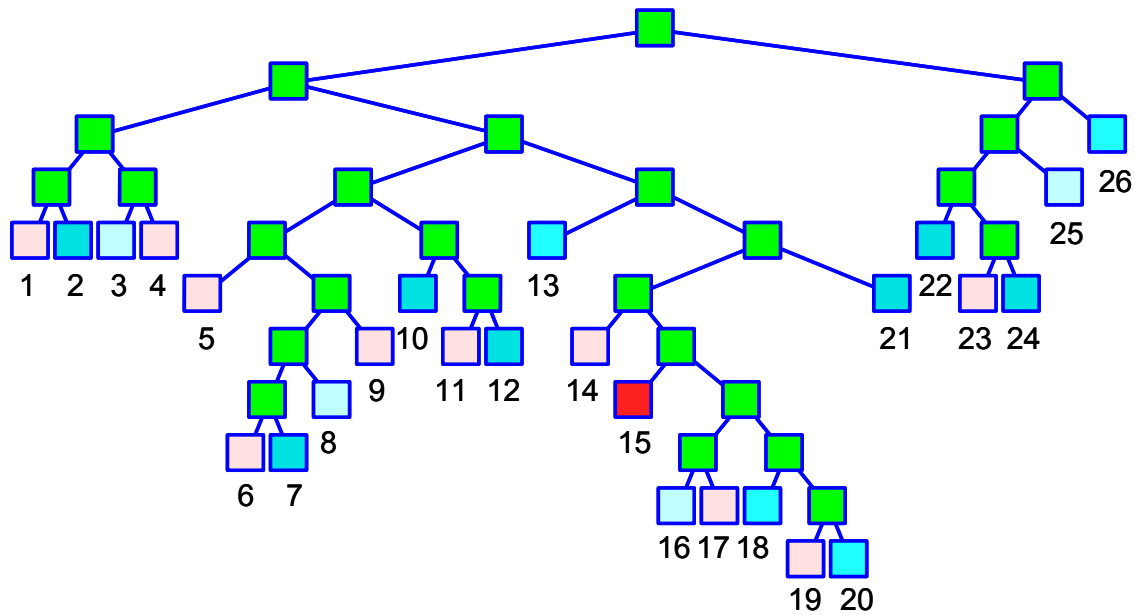


Figure 17. Forecast decision tree for Test 2, 10-fold cross-validation. A summary for each of the numbered nodes is provided in Table 9.

While 10-fold cross-validation may have provided improved misclassification errors, the forecast decision tree produced for this test was not an ideal decision tool, with a total of 26 terminal nodes as compared to 11 from Figure 15. Figure 17 depicts the

forecast decision tree produced from the Test 2 data. Due to the size of the tree, a modified version is shown, with the numerical node information provided in Table 15. A graph depicting the predictor variables used for splitting is shown in Figure 18.

Table 15. Terminal node details for Test 2 data set.

Terminal Node	Class Assignment	Node Purity Class 0	Node Purity Class 1	Number of Records Class 0	Number of Records Class 1
1	1	66.6%	33.4%	1045	523
2	0	96.9%	3.1%	31	1
3	0	90.8%	9.2%	337	34
4	1	65.8%	34.2%	79	41
5	1	72.1%	27.9%	588	227
6	1	80.9%	19.1%	178	42
7	0	100%	0%	19	0
8	0	90.4%	9.6%	179	19
9	1	68.7%	31.3%	46	21
10	0	97.5%	2.5%	236	6
11	1	76.3%	23.8%	61	19
12	0	100%	0%	28	0
13	0	93.4%	6.6%	694	49
14	1	72.5%	27.5%	87	33
15	1	33.3%	66.7%	3	6
16	0	90.5%	9.5%	95	10
17	1	69.4%	30.6%	59	26
18	0	93.9%	6.1%	170	11
19	1	75.9%	24.1%	63	20
20	0	92.1%	7.9%	58	5
21	0	97.1%	2.9%	101	3
22	0	100%	0%	25	0
23	1	77.2%	22.8%	258	76
24	0	100%	0%	19	0
25	0	91.3%	8.7%	230	22
26	0	95.4%	4.6%	2188	106

From studying Figure 18, it can be seen that the splitters at the top of the forecast decision tree match those evaluated with the initial decision trees: 1000DPD, 1000SPD,

and Deg C SST. This reaffirms the value of those parameters when forecasting fog for Kunsan AB. However, the decision tree is so complex, it would not be logical to use it for developing a simple forecast decision tool; therefore, the tree will be pruned upwards to determine if a more usable tree can be developed, without sacrificing misclassification rates.

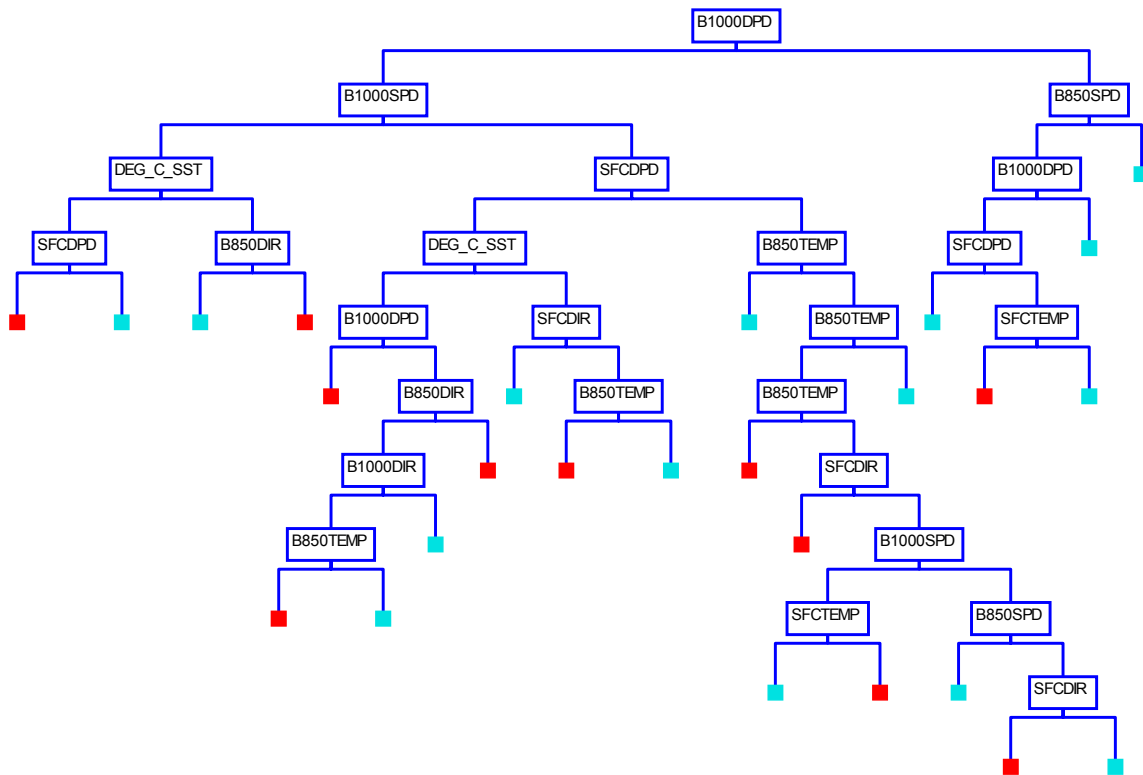


Figure 18. Predictor variables used for splitting Test 2 data with 10-fold cross-validation. The first three splits on the left side of the tree use the same variables as Figure 14 and 15.

The pruned forecast decision tree is shown in Figure 19, with the misclassification rates listed in Table 16. There was an increase in the percent of Class 1 misclassification

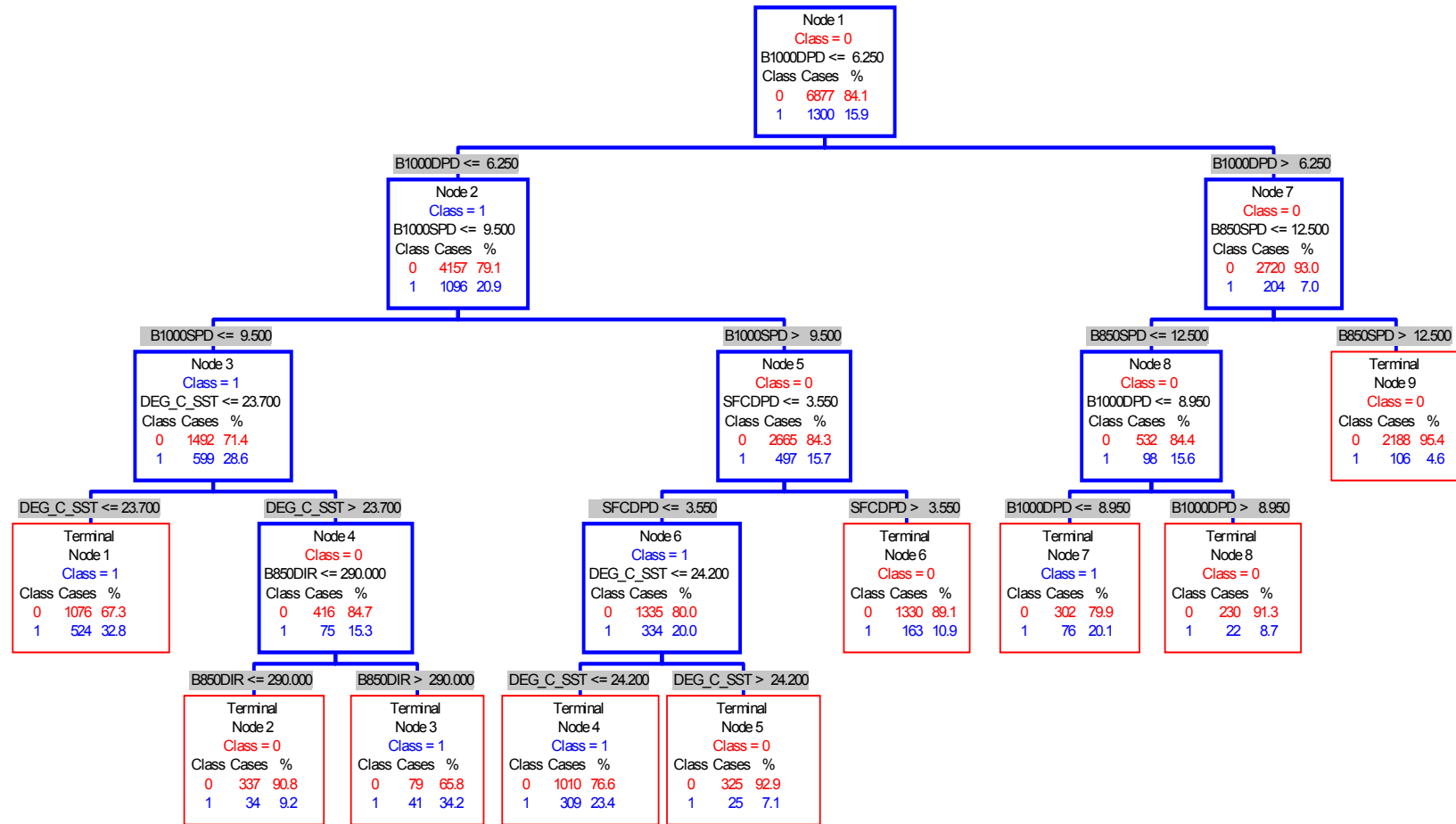


Figure 19. Pruned forecast decision tree from Test 2 data using 10-fold cross-validation. Relative costs increased from 0.645 to 0.663 with an increase in learn data set misclassification from 20.46% to 26.92%.

rates from 20.46% to 26.92%, which falls within the maximum target error of 30%. While this is tolerable, a more accurate decision tree is preferred for operational uses.

Table 16. Misclassification rates for pruned Test 2 data set, 10-fold cross-validation.

Class	Total Cases	Learn Data Error	Test Data Error	Learn Data Success	Test Data Success
0	6877	35.87%	37.21%	64.1%	62.8%
1	1300	26.92%	29.01%	73.1%	70.9%

5.2.3 Reclassified Sea Fog Target Variable. According to 607th Weather Squadron (2002), there are some wind directions at Kunsan that are more conducive to advective sea fog; it was determined it would be best to focus on those particular winds for the next test. For Kunsan AB, typically winds from the south through northwest result in the advection of sea fog into the operating area. Therefore, it was determined that reclassifying the Class 1 fog target variable could possibly lead to more accurate results. Going to the main data sheet, new criteria was established for the Class 1 target variable. In addition to visibility less than or equal to 4800 meters and present weather condition coded as BR, the surface winds reported at Kunsan AB must be from 140° to 340°. Only when all three of these criteria were met was the event classified as Class 1, and the data set relabeled “Test 3” (for all observations) and “Test 4” (removal of 0° through 135° upper air NOGAPS winds). This resulted in a reduction of Class 1 events from 2,026 to 876 from the initial data set, and 1,300 to 681 from the Test 2 data set. Due to the smaller number of Class 1 events, 10-fold cross-validation is the only method used for the following forecast decision trees.

Table 17 shows the results for the Test 3 classification tree, with a misclassification rate for learn data of 26.60% and test data of 30.25%, slightly out of the target 30% error rate range. These results are from the classification tree with the lowest relative costs. Further pruning of the tree yielded higher misclassification rates for the Class 1 sea fog events; therefore, pruning of this decision tree was not performed.

Table 17. Misclassification rates for Test 3 data set, 10-fold cross-validation.

Class	Total Cases	Learn Data Error	Test Data Error	Learn Data Success	Test Data Success
0	11710	36.06%	37.48%	63.9%	62.5%
1	876	26.60%	30.25%	73.4%	69.8%

The most significant feature to note from the forecast decision tree produced from the newly categorized target (Fig. 20) is the change in importance for the predictor variables. In the decision trees produced from the initial data set and Test 2 data, the primary parameters of interests were 1000DPD, 1000SPD and Deg C SST, regardless of the testing method employed. With the updated target variable, the most significant predictor variables are now 850TEMP, SFCDPD, SFCTEMP and 1000SPD. Using the JMP software program to run logistic stepwise regression tests on the new target variable yielded similar results. The top parameter considered by stepwise regression to be of importance when building the model is 850TEMP, which does match the results from CART. The other parameters determined by JMP in order of importance were Deg C SST, 1000DPD, 1000SPD and SFCTEMP. The order does differ from the CART output,

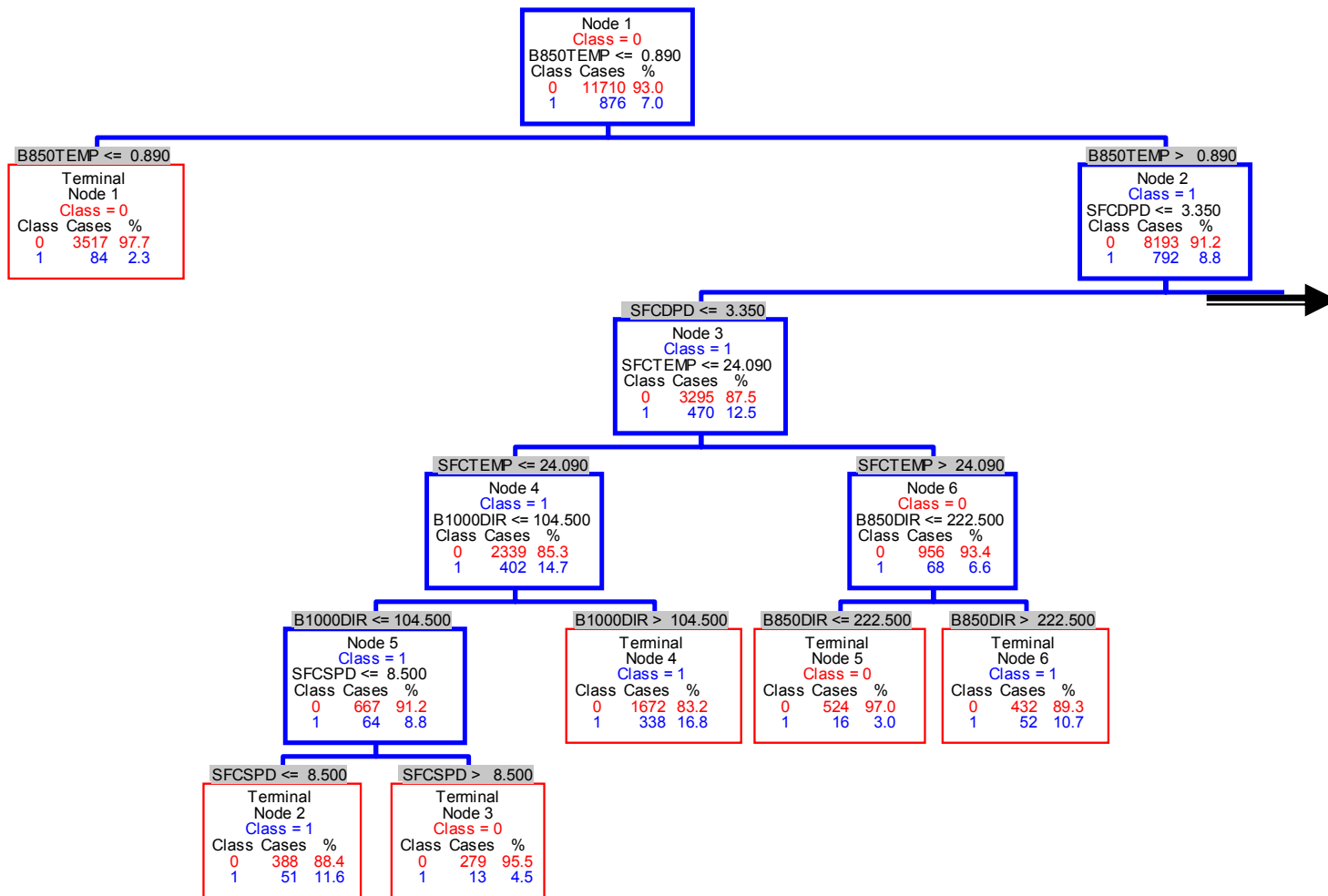


Figure 20. Forecast decision tree produced from Test 3 data, 10-fold cross-validation. This decision tree reclassifies the target, distinguishing all fog events from those events which are assumed to be specifically advective sea fog. Note that unlike prior decision trees, most of the Class 1 events now split to the right rather than the left of node 1.

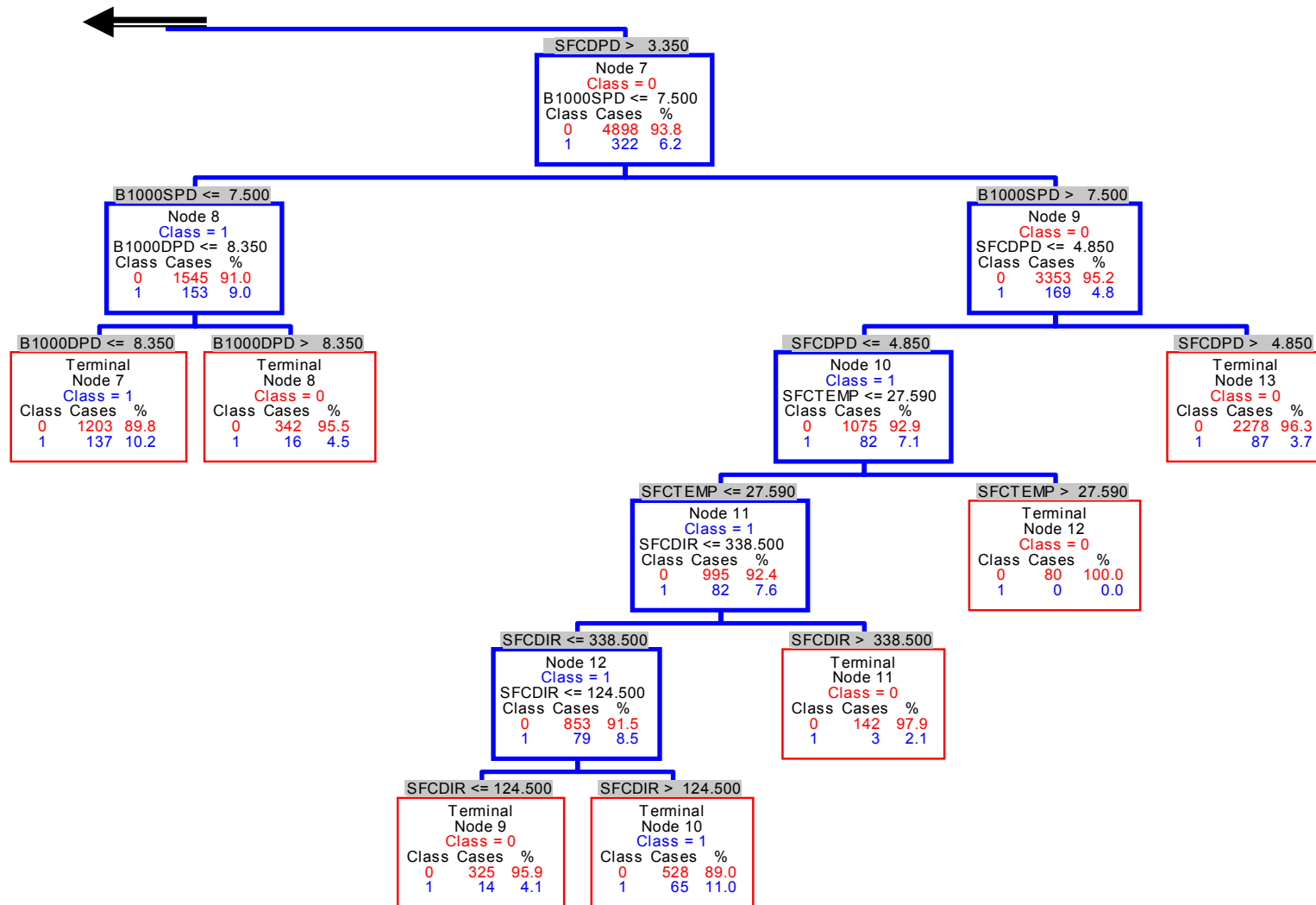


Figure 20. (Continued).

although SFCTEMP and 1000SPD are considered important predictors at the top of each model.

One thing to note when studying the number of Class 1 cases contained in the nodes is that some of them have a close to even split. For example, node 7 splits into node 8 and node 9 based on 1000SPD criteria. In this instance, 153 cases go to node 8, while 169 cases are split into node 9. With only a difference of 16 cases, this would seem to be relatively weak splitting criteria, with minor value to the research.

Another major limitation with this particular forecast decision tree is the wind direction splitting criteria. This particular data set maintained the original observational database, including wind directions from the complete 360° wind circle. This results in the same splitting weakness that occurred with the initial data set. Therefore, further testing was completed with the modified NOGAPS wind data.

Ten-fold cross-validation was performed on Test 4 data, sea fog events without NOGAPS winds from 0° to 135°. The relative cost for this decision tree was 0.597, the lowest of all the trees produced thus far. The misclassification results are displayed in Table 18, with the forecast decision tree in Figure 21, node report in Table 19, and splitting parameters in Figure 22.

Unlike the forecast decision tree produced from Test 3 data, it is possible to prune the Test 4 tree into a more manageable forecast tool, with minimal negative impacts to the misclassification rates. Table 20 shows the misclassification results for the pruned tree, with Figure 23 representing the pruned forecast decision tree.

Table 18. Misclassification rates for Test 4 data set, 10-fold cross-validation.

Class	Total Cases	Learn Data Error	Test Data Error	Learn Data Success	Test Data Success
0	7496	34.11%	32.52%	65.9%	67.5%
1	681	17.62%	27.17%	82.4%	72.8%

The learn data set for Test 4 has the lowest misclassification rate seen in the research, with 17.62% error. When running the test data against the forecast decision tree produced from the learn data sets, error increases to 27.17%, but still within the target of 30% maximum error. As with the forecast decision tree from Test 2, there are 18 terminal nodes which provides an unrealistic forecast decision tree for operational use. The tree is shown in Figure 21, with a report of the terminal node data given in Table 19.

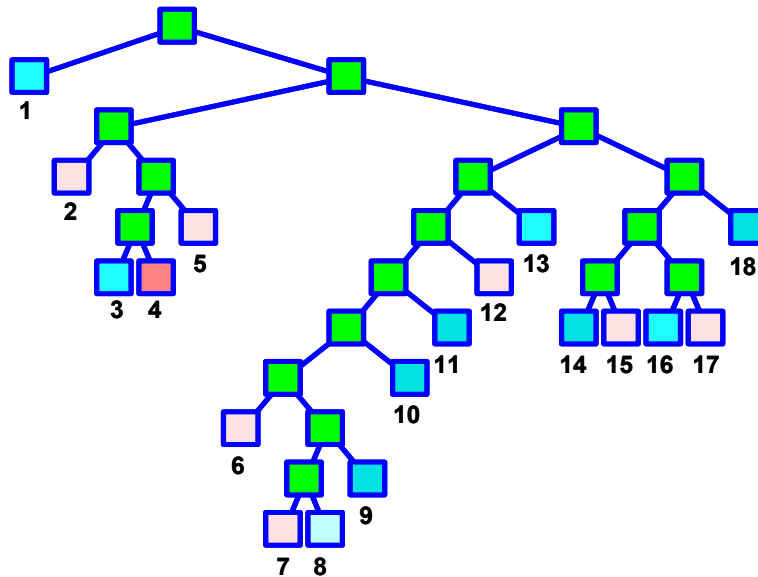


Figure 21. Forecast decision tree from Test 4 data, 10-fold cross-validation. A summary for each of the numbered nodes is provided in Table 13.

Table 19. Terminal node details for Test 4 data set.

Terminal Node	Class Assignment	Node Purity Class 0	Node Purity Class 1	Number of Records Class 0	Number of Records Class 1
1	0	97.8%	2.2%	2519	57
2	1	80.2%	19.8%	1425	352
3	0	97%	3%	558	17
4	1	66.7%	33.3%	8	4
5	1	84.4%	15.6%	76	14
6	1	88%	12%	309	42
7	1	88.2%	11.8%	180	24
8	0	95.3%	4.7%	204	10
9	0	98.9%	1.1%	90	1
10	0	100%	0%	53	0
11	0	98.4%	1.6%	121	2
12	1	81.9%	18.1%	384	85
13	0	96%	4%	333	14
14	0	100%	0%	37	0
15	1	82.1%	17.9%	165	36
16	0	97.6%	2.4%	249	6
17	1	71.4%	28.6%	10	4
18	0	98.4%	1.6%	775	13

The pruned forecast decision tree from Figure 23 reduces the number of nodes from the right side of the tree, while increasing the misclassification rate by less than two percent. This ensures the tree is more manageable as a decision tool, without sacrificing accuracy. From studying the tree, it is noted that node 2 contains a total of 624 Class 1 events, with a split of 387 into node 3 and 237 into node 4. Although there is a difference of 150 cases, the splitting criteria does not discriminate between classes well.

From node 3 the splitting criteria is $\text{DEG C SST} \leq 23.000$, resulting in a Class 1 terminal node 4. From the 237 Class 1 events in node 4, the split is 1000SPD to nodes 5 and 6, with a majority of the Class 1 events split into node 5. From node 5, the split

criteria is $\text{DEG_C_SST} \leq 23.000$ (same as node 3), with the majority of Class 1 events forming terminal node 4. Similar terminal node results for DEG C SST from different branches of the decision tree allow a workable solution to the previously mentioned node 2 split.

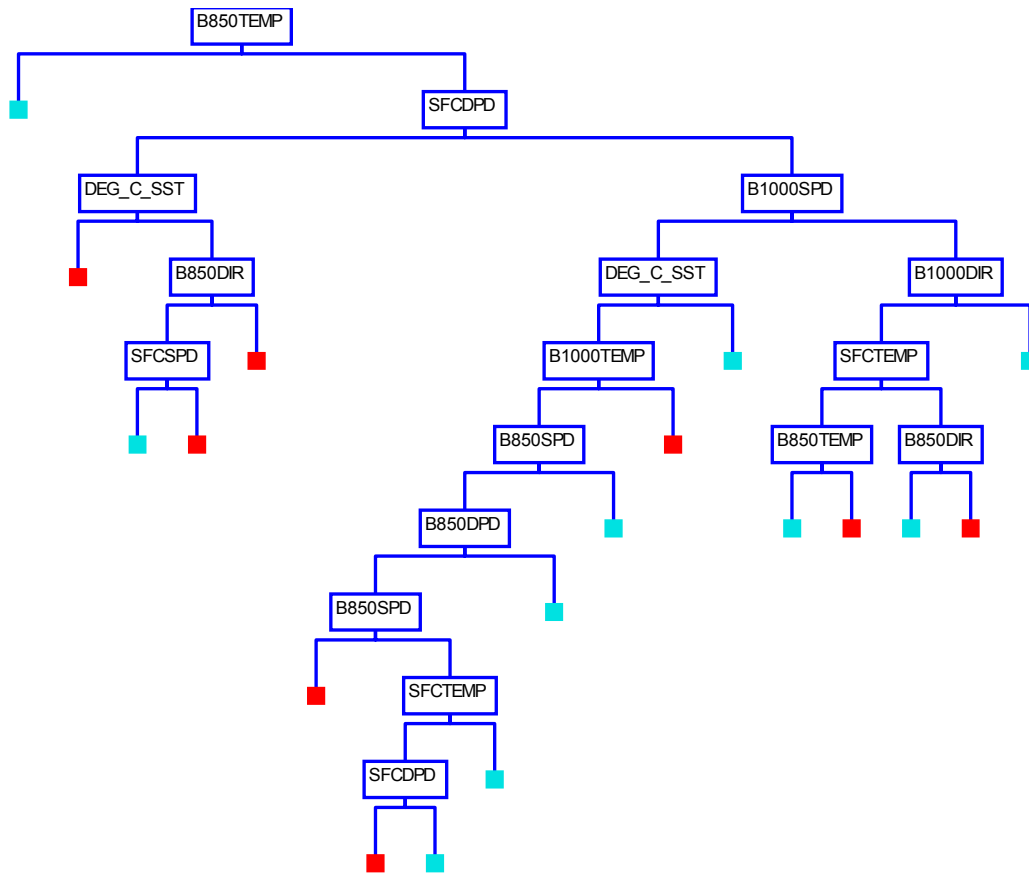


Figure 22. Predictor variables used for splitting Test 4 data with 10-fold cross-validation. Note that the first two splits of the decision tree use the same predictor variables as the Test 3 decision tree in Figure 20.

Table 20. Misclassification rates for pruned Test 4 data set, 10-fold cross-validation.

Class	Total Cases	Learn Data Error	Test Data Error	Learn Data Success	Test Data Success
0	7496	35.59%	34.99%	60.4%	65.0%
1	681	18.94%	28.63%	81.1%	71.4%

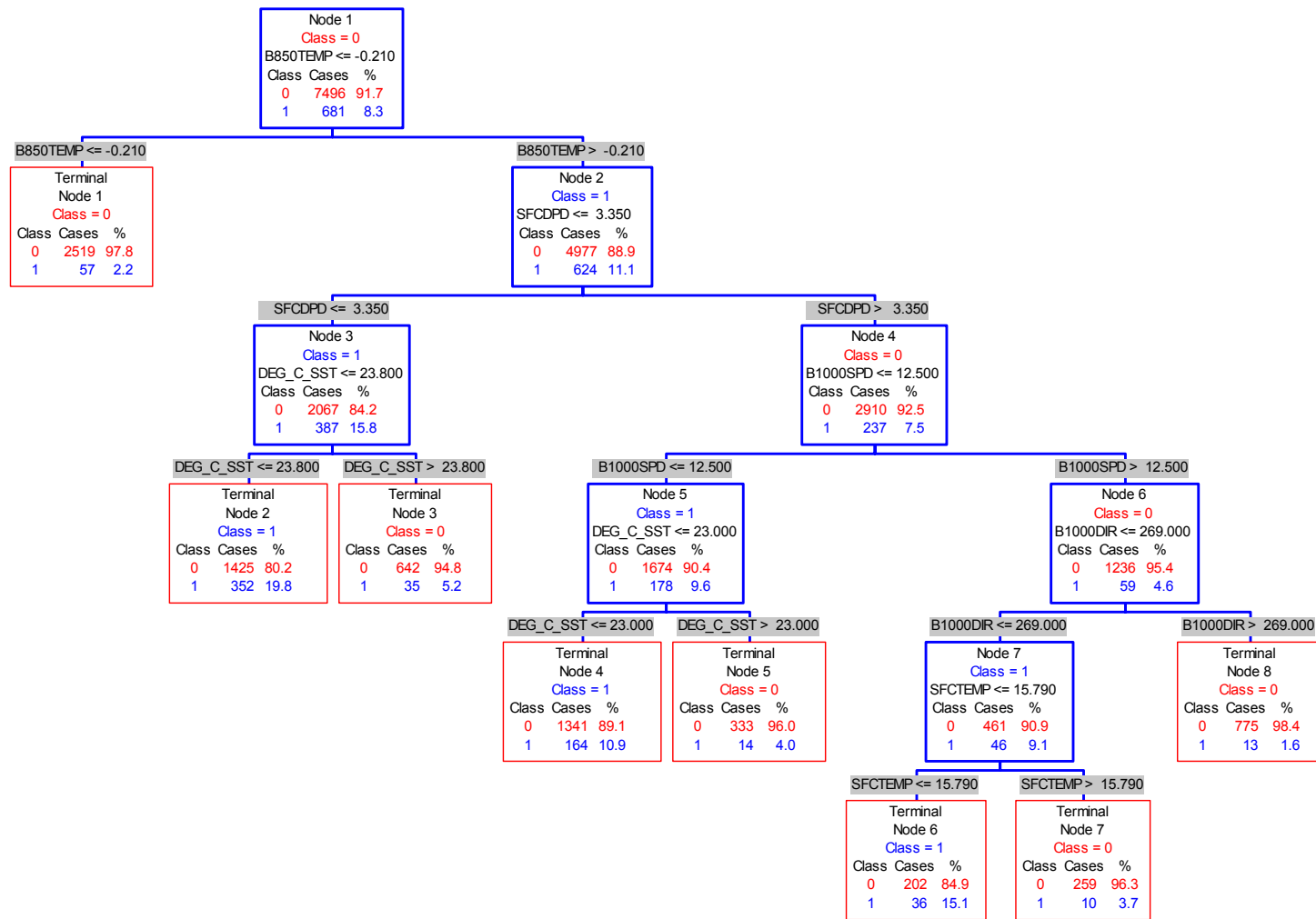


Figure 23. Forecast decision tree from pruned Test 4 data, 10-fold cross-validation. Note that the split from node 2 to nodes 3 and 4 only has a difference of 150 cases, resulting in a close split. It would seem that while SFCDPD is a split criterion, it is not a very decisive parameter.

5.2.4 Addition of new predictor variables. One more test was conducted using the Test 4 data set, with the addition of two new predictor variables. According to Cho et al. (2000), the difference between air temperature (AT) and SST, as well as the difference between dew point (DP) and SST are important factors that affect the occurrence of sea fog. These two parameters were calculated in the datasheet and run through the CART program, using Gini and 10-fold cross-validation. The first forecast decision tree produced has a relative cost of 0.604 and a total of 24 terminal nodes. The misclassification rates are shown in Table 21, with the decision tree displayed in Figure 24, node report in Table 22, and splitter variables in Figure 25.

Table 21. Misclassification rates with AT-SST and DP-SST predictor variables.

Class	Total Cases	Learn Data Error	Test Data Error	Learn Data Success	Test Data Success
0	7496	31.96%	33.50%	68.0%	66.5%
1	681	17.62%	26.87%	82.4%	73.1%

Table 21 lists a misclassification rate for Class 1 events as 17.62% for learn data and 26.87% for test data, which is similar to the rates calculated for the sea fog Test 4 data. Figure 24 shows there are 24 terminal nodes in the optimal tree, which makes this an unrealistic tool for use in forecasting sea fog events. Figure 25 shows the splitting variables used for the new decision tree. Although the misclassification rates are similar from this test and the Test 4 data set, there is a significant difference in the splitting variables from Figure 25 to those from Figure 22. The new predictor variable DP-SST located in node 1 is now the primary splitter for the data set.

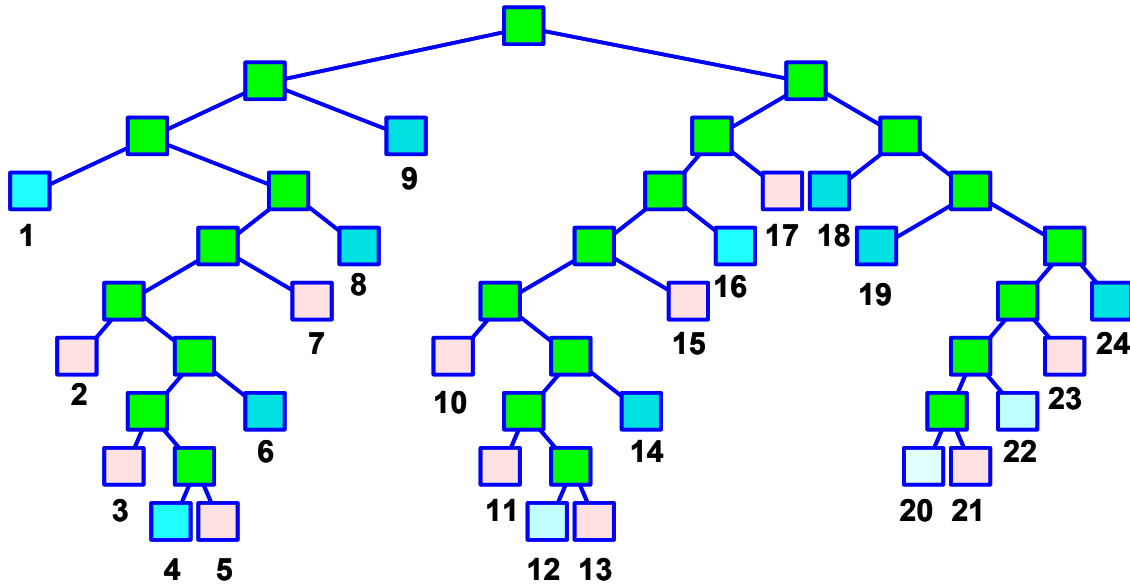


Figure 24. Forecast decision tree with AT-SST and DP-SST predictor variables. A summary for each of the numbered terminal nodes is provided in Table 16.

From reviewing the results from this latest test, the misclassification rates are acceptable for developing a forecast tool, but the tree itself has too many terminal nodes for adequate operational use. Therefore, the tree was pruned back to reduce the number of nodes, and providing a reasonable forecast decision tree with the new predictor variables. By pruning the tree upwards, the relative cost increased from 0.604 to 0.644, but the Class 1 misclassification results did not differ significantly from the optimal tree, as shown in Table 23.

The Class 1 test data error has an increase of near one percent for the pruned tree. By using this particular forecasting decision tree, there is approximately a test data 72% prediction success rate for forecasting advective sea fog for Kunsan AB. The decision tree with the new predictor variables is shown in Figure 26.

Table 22. Terminal node details with new AT-SST and DP-SST predictor variable.

Terminal Node	Class Assignment	Node Purity Class 0	Node Purity Class 1	Number of Records Class 0	Number of Records Class 1
1	0	96.5%	3.5%	495	18
2	1	78.6%	21.4%	33	9
3	1	79.5%	20.5%	31	8
4	0	97.7%	2.3%	129	3
5	1	88%	12%	73	10
6	0	100%	0%	73	0
7	1	78.2%	21.8%	154	43
8	0	99.1%	4.7%	204	10
9	0	98.5%	1.5%	2605	41
10	1	83.8%	16.2%	109	21
11	1	81.8%	18.2%	45	10
12	0	94.9%	5.1%	409	22
13	1	70.6%	29.4%	12	5
14	0	100%	0%	75	0
15	1	81.1%	18.9%	163	38
16	0	97.4%	2.6%	227	6
17	1	81.3%	18.7%	1686	388
18	0	98.2%	1.8%	430	8
19	0	99.1%	0.9%	106	1
20	0	93.7%	6.3%	149	10
21	1	76.8%	23.2%	63	19
22	0	95.8%	4.2%	227	10
23	1	73%	27%	27	10
24	0	100%	0%	66	0

Studying the pruned decision tree from Figure 26 shows that the predictor variable DP-SST is now the lead splitting criterion, as compared to 850TMP from Figure 23. The second split of importance for Class 1 events was Deg C SST, which already proved to be a significant variable as shown in previous decision trees.

Reviewing all the tests and forecast decision trees produced for this research problem, it is determined that the two most significant for the forecasting of sea fog are the trees from Figure 23 and Figure 26. These two decision trees come from a data set

that had been filtered to remove winds that did little to contribute to the development of sea fog. In addition, the target variable was formatted from the Kunsan AB surface observations in a way such that the reduced visibility events that were not the direct result

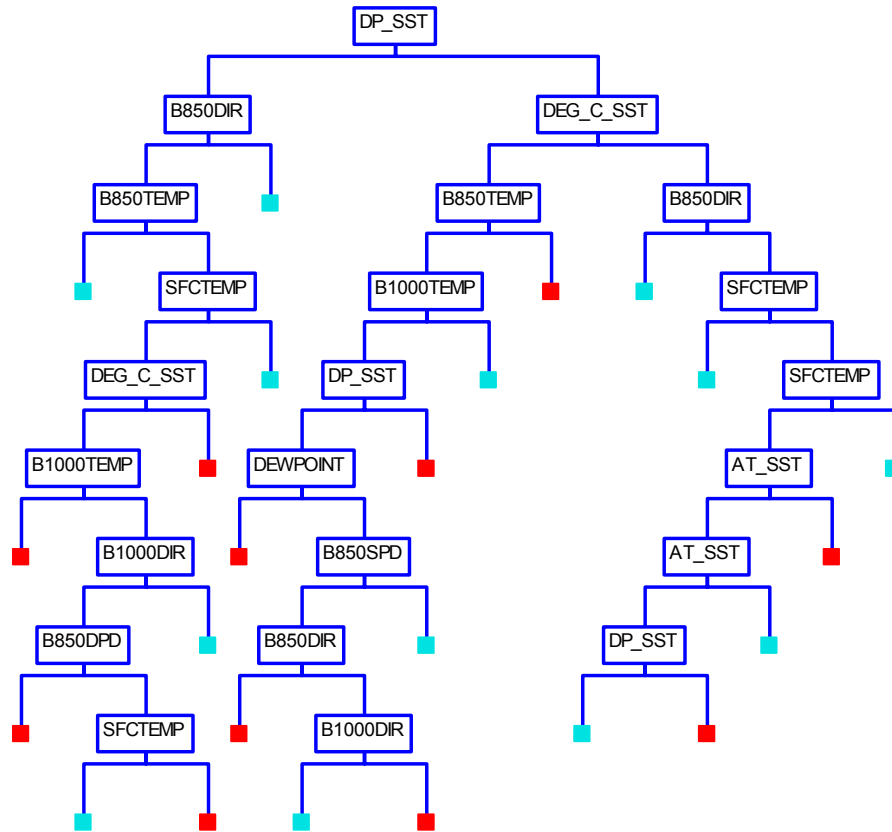


Figure 25. Forecast decision tree splitters with new predictor variables. Note that the primary split is based on the new variable DP-SST, while AT-SST is further down the right side of the tree.

Table 23. Misclassification rates for pruned tree with AT-SST and DP-SST variables.

Class	Total Cases	Learn Data Error	Test Data Error	Learn Data Success	Test Data Success
0	7496	39.91%	36.21%	60.1%	63.8%
1	681	18.21%	28.19%	81.8%	71.9%

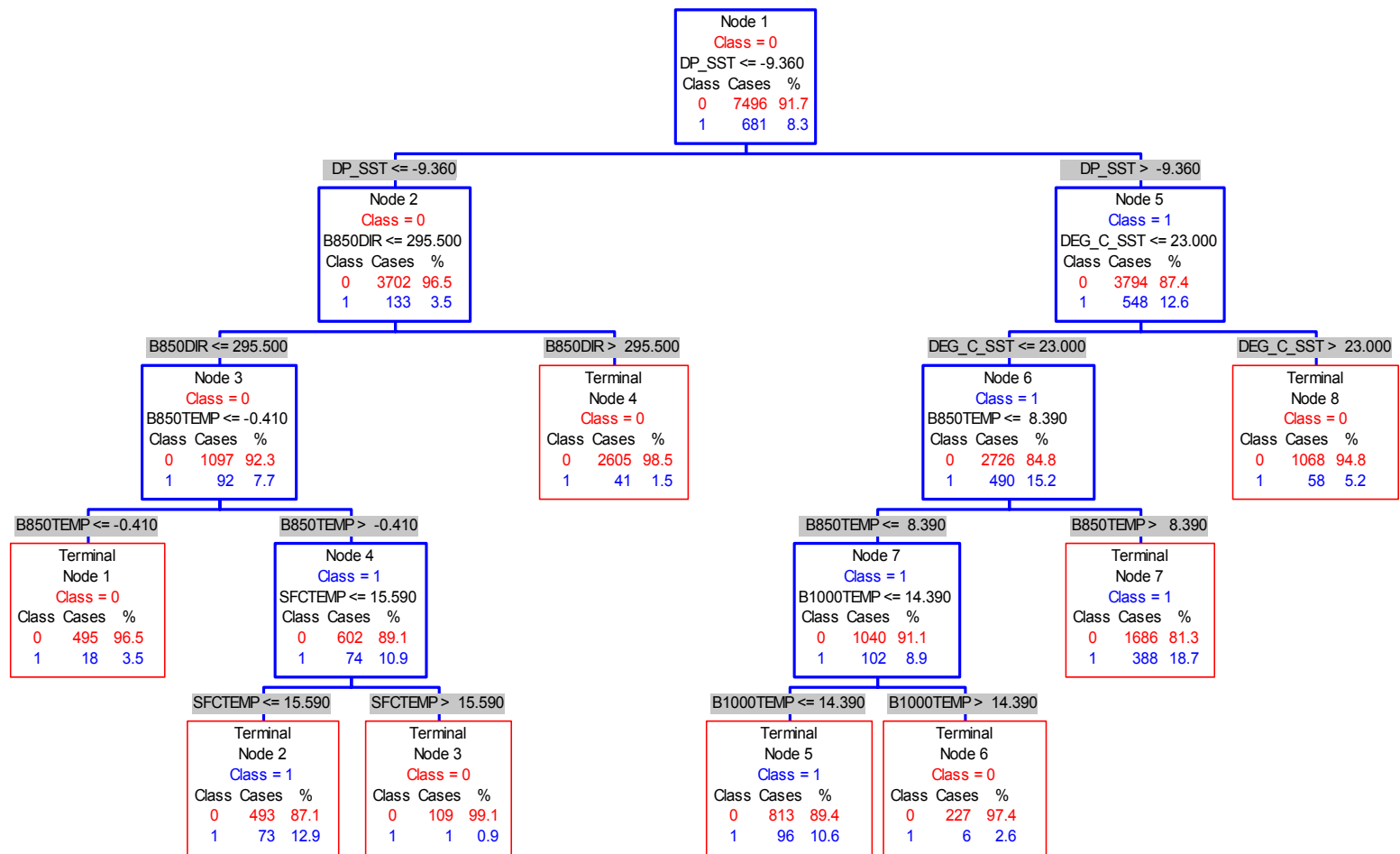


Figure 26. Forecast decision tree with AT-SST and DP-SST predictor variables. Note that the new variable DP-SST is the splitting criterion for node 1, with a majority of Class 1 events moving into the right side of the decision tree.

of sea fog were not classified as Class 1 events. Finally, these two particular trees had the lowest misclassification results for Class 1 events when compared to all the tests conducted.

The splitting rules established for the produced trees are to be verified with 24-hour lead-time of the occurrence of sea fog at Kunsan AB. These rules have been established through the CART program with 10 years of climatological analysis data. The predictors yield a 72% accuracy rating, and should be used as a guide for a more sound forecast decision of sea fog 24 hours in advance.

VI. Conclusions and Recommendations

6.1 Conclusions

The overall goal of this research was to determine a method for forecasting sea fog events at Kunsan AB, with a 24-hour lead-time. The primary method used to satisfy this objective was data mining with classification and regression tree analyses. This research used observational data from Kunsan AB and analysis data from the NOGAPS and SFCTMP models covering the Yellow Sea region.

The first objective was to perform a geographical and climatological overview of the Kunsan AB region. Kunsan is a port city located in southwest Korea, bordered on the west and south by the Yellow Sea. The close proximity to the water and seasonal fluctuations of the Yellow Sea Current result in numerous advective sea fog events in the area, particularly in the spring and summer months when cold water upwelling is prevalent.

The second objective defined fog types and formation processes, and how they relate to this region. The formation of sea fog is dependent on hydrological factors such as sea current and sea surface temperature, as well as air temperature, humidity, and wind. Advective sea fog is formed when warmer air moves over a cooler water surface, such as when warmer air moves over the cold water upwelling off the coasts of southwest Korea.

Third, the collection of sea surface temperature data, upper air data, and surface observational data for Kunsan AB, as well as upstream locations (both over land and the Yellow Sea), was necessary to continue the study. The three sets of data included surface weather observations for Kunsan AB, sea surface temperature data for the Yellow

Sea (both obtained from AFCCC databases), and upper air grid data for the Yellow Sea region covering four grid points (from the NOGAPS model).

For the fourth objective, formatting all the data was necessary in order to perform statistical examinations. Since the target variable was defined categorically, logistic regression (which works with a binary outcome variable) was the statistical method of choice. These tests compared the correlation between the target variable (sea fog) and the various predictor variables. Stepwise logistic regression was performed on JMP to determine the importance of various predictor variables. The study was narrowed down to one grid point of interest, which from initial testing had the most significant effect on advective sea fog impacting Kunsan AB. The predictors were listed in order of importance to the formation of fog, but more detailed information was needed to provide a forecast decision tool to the 8th OSS/OSW at Kunsan AB.

To develop a forecast decision tool, the fifth objective was to use data mining CART analysis on the data sets. Data mining was used to determine if there were relationships between the target variable and predictor variables that was not evident through standard statistical regression. Multiple tests were run, modifying the data sets in an effort to produce the most effective forecast tool. The predictor variables used for splitting in the initial forecast decision trees were similar to those variables determined by JMP to be of most importance: 1000DPD, 1000SPD, DEG C SST, and 850DPD. Upon changing the rules for categorizing the target variable, the key parameter of importance as determined by JMP was 850TMP, which was the same result as the decision tree produced by CART. A final test was performed by adding two new predictor variables, which once again changed the splitting criteria. One of the new

variables, DP-SST was listed as the most significant in JMP, as well as the top splitting criterion in CART.

The final objective was to develop forecast decision trees to assist in choosing the best predictors for forecasting advective sea fog, and providing that product to the 8th OSS/OSW at Kunsan AB. Beginning with the initial data set and eventually modifying the target variable and adding two new predictors, a total of nine forecast decision trees were produced.

The first decision tree produced a test data accuracy rating of 65.4%, well below the standards set for this research. Upon modifying the wind data, the accuracy rating for test data increased to 71.2%. The next decision tree of importance contained the reclassified target variable, and produced an accuracy rating of 72.8%, but this tree was too large to use operationally without producing a computerized forecast model. Upon pruning the tree (Figure 23), the accuracy rating decreased to 71.4%, but still within reasonable limits. A final tree was developed by adding two predictor variables and pruning upwards (Figure 26), yielding an accuracy rating of 71.9%. It was determined that the decision trees from Figure 23 and Figure 26 produced the best results, with an almost equal prediction success of approximately 72%.

The forecast decision trees from Figures 23 and 26 contained the data set that removed observations with SFCDIR, 1000DIR, and 850DIR NOGAPS values between 0° and 135°, which accounted for 35 percent of the total data set, and 36 percent of all fog events (including radiation fog events). In addition, the target variable was reclassified from the original “Fog \leq 4800” to “Sea Fog”, which had the following conditions: visibility less than or equal to 4800 meters, present weather condition coded

as BR, and the surface winds reported at Kunsan AB from 140° to 340°. This was done in an effort to filter radiation fog events rather than advection sea fog occurrences.

It was determined to make two sea fog decision tree tools; one based off of each of the selected CART forecast decision trees. Since each of the selected decision trees produced an accuracy rating of approximately 72%, both should be tested for application in real-time weather forecasting. The final Sea Fog Forecast Decision Trees are seen in Appendices A and B. These rules are experimental and formulated as suggestive criteria for developing more accurate sea fog forecasts. However, they are provided and recommended for immediate operational use as they are developed from actual observational data.

6.2 Recommendations

CART analyses used in this research provided insightful information into the feasibility of providing forecasts by means of forecast decision trees. Given large databases and a variety of predictors, accuracy ratings can be calculated for new methods in forecasting which may not have been considered previously. However, given the nature of data mining and as seen from the products produced in this research, CART does not always yield one unambiguous method which can be used in forecast decisions.

Further research on this particular topic is desired in an effort to improve accuracy ratings of the forecast decision trees. An extended POR will yield a greater database for CART to work with, allowing a wider range of tests to be conducted within the program, rather than just 10-fold cross-validation. In addition, the NOGAPS data used for this research was on a 2.5 x 2.5 degree grid, whereas NOGAPS is now available on a 1 x 1 degree grid. A wider range of data points in the region to the west of Kunsan

AB may provide a more accurate location from which to forecast the formation of advective sea fog events.

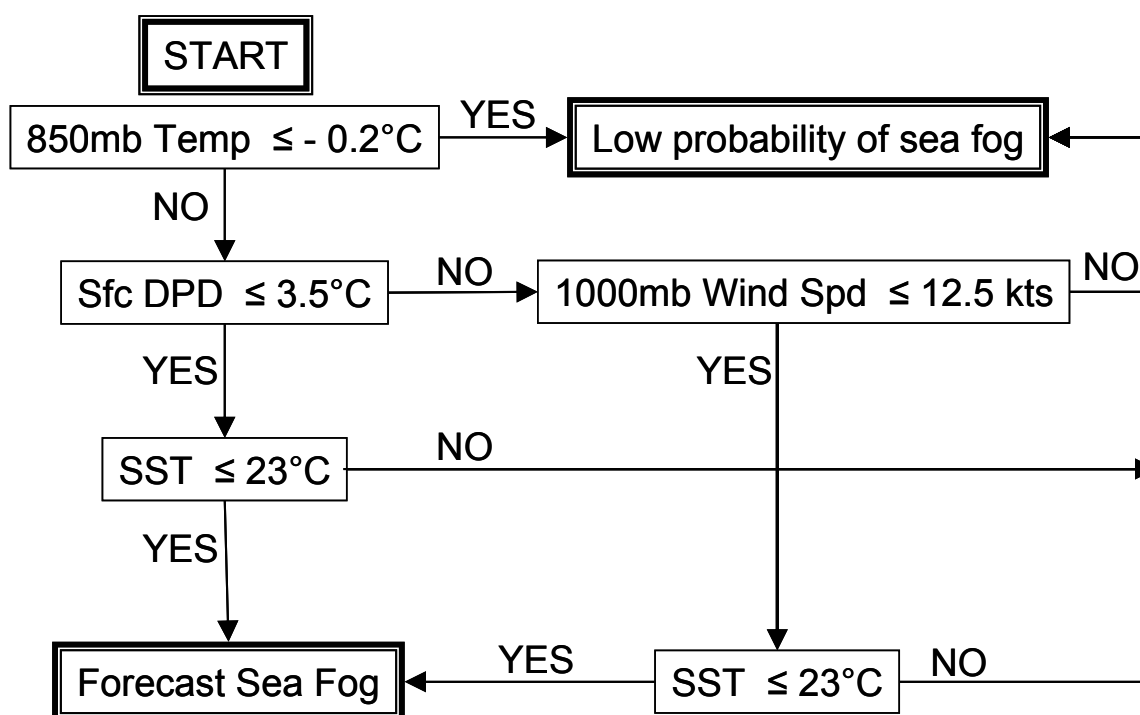
Another recommendation for future research is to develop the forecasting decision tree to include low level stratus conditions in addition to sea fog advecting into the Kunsan operating area. On many occasions low stratus accompanies sea fog events, with both having negative impacts to military air operations, and should be considered in future forecast decision trees.

Throughout this project, accuracy ratings were sacrificed in order to produce forecast decision trees that are easy for a forecaster to follow. In the future, the potential to automate the process into a computer program will allow the use of the complete decision trees without pruning. This would produce higher accuracy ratings for sea fog forecasting, as well as provide a means for an easily generated model output statistic.

It is recommended that further weather research can be conducted in CART, provided sufficient data and an ample POR is available for any potential study. There are numerous ways to approach data analyses with this program, with a goal of maintaining a low misclassification rate. Overall, CART provided useful information as to which predictors can be used to forecast the arrival of advective sea fog into the Kunsan AB area with 24-hour notification. Further evaluation and refining of the decision trees provided should be conducted, so this method can be included into the important forecast process.

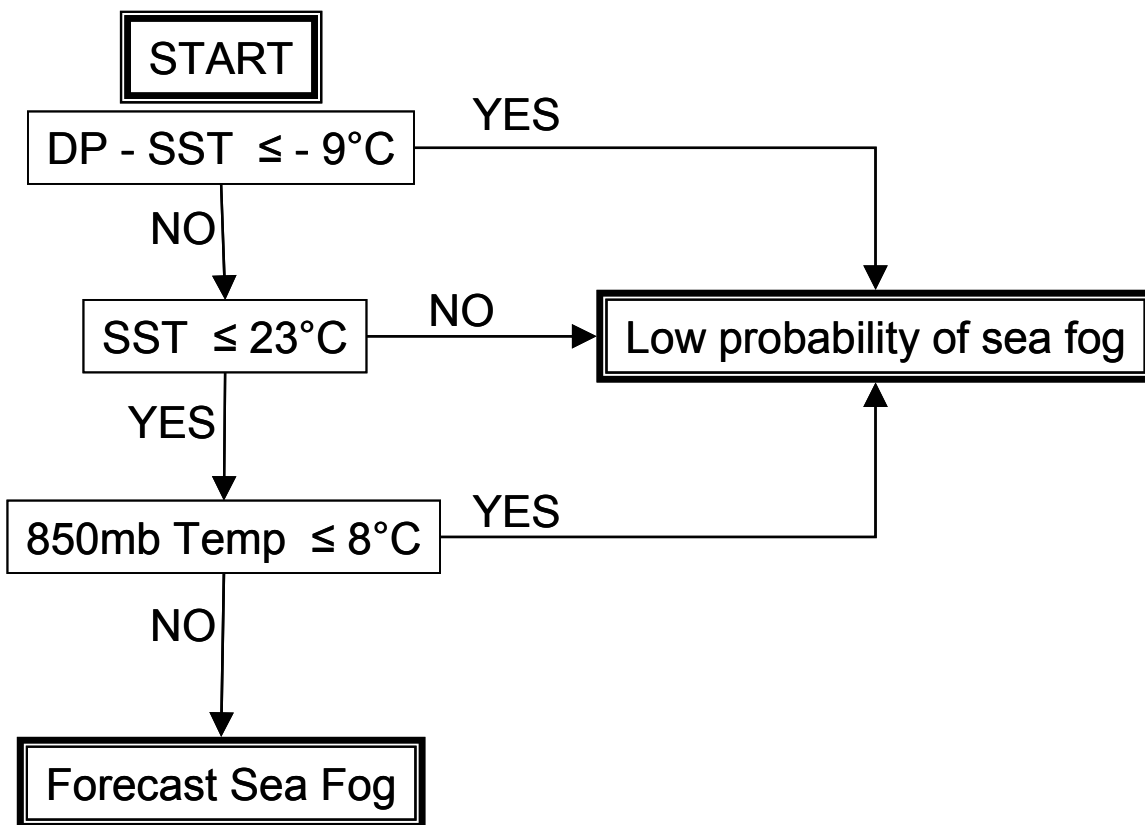
Appendix A: Decision Tree #1 for Forecasting Sea Fog at Kunsan AB

This is a forecast decision tree based off the CART tree produced in Figure 23. This graph is provided as a supplemental tool for forecasting the formation of sea fog, and was designed to be applied for the location at 125E 35N. The lead time for this tree is 24 hours; therefore, these are the conditions that should exist at that NOGAPS model grid point 24 hours prior to the formation of sea fog. If the parameters indicate “Forecast Sea Fog”, use the Land/Sea Breeze Front Checklist (Appendix C) developed by the 607th Weather Squadron (2002) to determine if there will be a sea breeze. If yes, it is likely there is a high probability sea fog will advect into the Kunsan AB area.



Appendix B: Decision Tree #2 for Forecasting Sea Fog at Kunsan AB

This is a forecast decision tree based off the CART tree produced in Figure 26. This graph is provided as a supplemental tool for forecasting the formation of sea fog, and was designed to be applied for the location at 125E 35N. The lead time for this tree is 24 hours; therefore, these are the conditions that should exist at that NOGAPS model grid point 24 hours prior to the formation of sea fog. If the parameters indicate to “Forecast Sea Fog”, use the Land/Sea Breeze Front Checklist (Appendix C) developed by the 607th Weather Squadron (2002) to determine if there will be a sea breeze. If yes, it is likely there is a high probability sea fog will advect into the Kunsan AB area.



Appendix C: Land/Sea Breeze Front Checklist

This land/sea breeze checklist was obtained from the 607th Weather Squadron (2002). It is recommended for use when forecasting the advection of sea fog into Kunsan AB.

1. Sea surface temperature (SST) near area of interest. _____(°C)
2. Land temperature (LT) required today (SST + 3.5°C) (see below). _____(°C)
3. Maximum temperature expected today. _____(°C)
4. Is temperature favorable? If the value in step 2 is less than in step 1, enter NO.
If it is the same or more, enter YES. YES/NO
5. Wind direction at 0900L today. _____(deg)
6. Is direction favorable? If it is from sea to land, enter NO.
If it is from land to sea or is calm, enter YES. YES/NO
7. Wind speed at 0900L today. _____ (knots)
8. Is speed favorable? If it is more than 9 knots, enter NO. If it is 9 knots or less, enter YES.
YES/NO
9. Will a sea breeze pass the station today? If NO has been answered for any step above, enter NO.
If YES has been answered for steps 3, 5, and 7, enter YES. YES/NO

This table was developed using a monthly mean sea surface temperature plus 3.5 Celsius degrees. The table does not take into account the daily variations in SST each month. Temperatures are in degrees Celsius.

Month	Land temp required for sea breeze (deg C)
January	10
February	8
March	10
April	13
May	16
June	20
July	24
August	28
September	25
October	21
November	16
December	12

ACRONYMS

AFCCC	Air Force Combat Climatology Center
AFGWC	Air Force Global Weather Central
AFWA	Air Force Weather Agency
AT	Air Temperature
BR	Mist
C	Celsius
CART	Classification and Regression Tree
DP	Dew Point
DPD	Dew Point Depression
FAA	Federal Aviation Administration
FG	Fog
FNMOCC	Fleet Numerical Meteorology and Oceanography Center
K	Kelvin
LST	Local Standard Time
METAR	Aviation Routine Weather Reports
NOGAPS	Navy Operational Global Atmospheric Prediction System
OCDS	Operational Climatic Data Summary
OI	Optimum Interpolation
OSS/OSW	Operational Support Squadron Weather Flight
POR	Period of Record
QC	Quality Control

RAOB	Rawinsonde Observation
ROK	Republic of Korea
RTNEPH	Real-Time Nephanalysis Model
SFCTMP	Surface Temperature Model
SST	Sea Surface Temperature
TEMP	Temperature
WS	Weather Squadron
WW	Weather Wing

Bibliography

- 5th Weather Wing, 1979: *Fog and Stratus*. 5 Weather Wing (5 WW)/Field Manual-79/001, 8 pp.
- 607th Weather Squadron (WS), 1998: *Korean Theater Weather Support and Climatology*. 607 WS Pamphlet 15-5, 198 pp.
- 607th Weather Squadron, 2002: *Korean Theater Weather Support and Climatology*. 607 WS Pamphlet 15-5, 287 pp.
- Ahrens, Donald C., 1994: *Meteorology Today: An Introduction to Weather, Climate, and the Environment*. Fifth Edition. West Publishing Company. 592 pp.
- Air Force Manual (AFMAN) 15-111, *Surface Weather Observations*, HQ AFWA/XOW, 18 September 2001.
- Benz, Richard F. "Data Mining Atmospheric/Oceanic Parameters in the Design of a Long-Range Nephelometric Forecast Tool," Master's Thesis, Air Force Institute of Technology, Department Engineering Physics, 42-47, 2003.
- Binhua, Wang, 1985: *Sea Fog*. China Ocean Press. 330 pp.
- Breiman, L.; Friedman, J.H., Olshen, R.A. and Stone, C.J., 1984: *Classification and Regression Trees*. Wadsworth, Belmont, CA, 358 pp.
- Cho, Yang-Ki, Kim, Moon-Ouk, and Kim, Byung-Choon, 2000: Sea Fog and the Korean Peninsula. *Journal of Applied Meteorology*, **39**, 2473-2479.
- Department of the Air Force. *Surface Temperature Analysis*. USAF Environmental Technical Applications Center Climatic Database, Users Handbook 86, No. 2, October 1986.
- Department of the Air Force. *HIRAS: USAFETAC Climatic Database*. USAF Environmental Technical Applications Center Climatic Database, Users Handbook 88/001, No. 5, February 1991.
- Federal Aviation Agency and Department of Commerce, 1965: *Aviation Weather for Pilots and Flight Operations Personnel*. Superintendent of Documents, US Government Printing Office, Washington DC, 299 pp.
- Glickman, T.S., 2000: *Glossary of Meteorology*. American Meteorological Society, 855 pp.

- Guttman, N. B., 1971: *Study of Worldwide Occurrence of Fog, Thunderstorms, Supercooled Low Clouds and Freezing Temperatures*. U.S. Naval Weather Service Command, NAVAIR 50-1C-60, 67 pp.
- Hosmer, David W., and Lemeshow, Stanley, 2000: *Applied Logistic Regression*. Second Edition. John Wiley and Sons, Inc., 375 pp.
- Kopp, Thomas J., 1995: *The Air Force Global Weather Central Surface Temperature Model*. Air Force Global Weather Central Technical Note 95/004, 23 pp.
- Koschmeider, H., 1924: *Beitr. Phys. Freien Atmosphere*, **12**, 33-35 and 171-181.
- Lewis, Roger J., 2000: *An Introduction to Classification and Regression Tree (CART) Analysis*. Department of Emergency Medicine, Harbor-UCLA Medical Center, Torrance, CA.
- Microsoft Encarta® Encyclopedia, 2001. *South Korea*. 1993-2000 Microsoft Corporation.
- Neiburger, M., and Wurtele, M. G., 1949: *Chem. Rev.*, **44**, 321-335.
- Orgill, Montie, 1993. *An Examination of the Evolution of Radiation and Advection Fogs*. Science and Technology Corporation, White Sands Missile Range, New Mexico, ADA266127, 68 pp.
- Petterssen, Sverre, 1956: *Weather Analysis and Forecasting, 2nd Edition. Volume II: Weather and Weather Systems*. McGraw-Hill Book Co., New York, 266 pp.
- Roach, W.T., 1995: Back to Basics: Fog Part 3—The Formation and Dissipation of Sea Fog. *Weather*. 50, 80-84.
- Salford Systems, 2001: *CART®: Tree Structured Non-Parametric Data Analysis*. San Diego, CA, 355 pp.
- Salford Systems, 2002: *An Implementation of the Original CART Method*. San Diego, CA, 308 pp.
- SAS Institute, 2000. *JMP Statistics and Graphics Guide*. SAS Institute Inc., Cary, NC, 634 pp.
- Steinberg, D. and Colla, P., 1995: *CART: Tree-structured nonparametric data analysis*. San Diego, CA: Salford Systems, 355 pp.

- Venne, Monique G., Jasperson, William H., and Venne, David E., 1997: *Difficult Weather: A Review of Thunderstorm, Fog and Stratus, and Winter Precipitation Forecasting*. Center for Atmospheric and Space Sciences PL-TR-97-2125, 48 pp.
- Wallace, John M., and Hobbs, Peter V., 1977: *Atmospheric Science: An Introductory Survey*. Academic Press. 467 pp.
- Wilks, Daniel S., 1995: *Statistical Methods in the Atmospheric Sciences*. Academic Press, Inc., 467 pp.

Vita

Captain Danielle M. Lewis graduated from Nathan Bedford Forrest High School in Jacksonville, Florida. She entered undergraduate studies at the University of South Alabama, Mobile, Alabama where she graduated with a Bachelor of Science degree in Geography-Meteorology. She was commissioned through Operating Location 432a AFROTC at the University of South Alabama where she was recognized as a Distinguished Graduate.

Her first assignment was at Keesler AFB, Mississippi as a student in the Weather Officers Course. She was then assigned to the 347th Operational Support Squadron, Moody AFB, Georgia, where she served as the Wing Weather Officer. While stationed at Moody, she deployed to Panama, providing weather support to the Joint Inter-Agency Task Force South. She was assigned to Detachment 11, 7th Weather Squadron, supporting US Army V Corps in Heidelberg, Germany, and serving a deployment in Bosnia-Herzegovina during that time. She moved to HQ 7th Weather Squadron in the position of Chief, US Army Europe Support. She was selected to attend the Graduate Meteorology program, Department of Engineering Physics, Air Force Institute of Technology. Upon graduation, she will be assigned to Offutt AFB, Nebraska.

REPORT DOCUMENTATION PAGE				Form Approved OMB No. 074-0188	
<p>The public reporting burden for this collection of information is estimated to average 1 hour per response, including the time for reviewing instructions, searching existing data sources, gathering and maintaining the data needed, and completing and reviewing the collection of information. Send comments regarding this burden estimate or any other aspect of the collection of information, including suggestions for reducing this burden to Department of Defense, Washington Headquarters Services, Directorate for Information Operations and Reports (0704-0188), 1215 Jefferson Davis Highway, Suite 1204, Arlington, VA 22202-4302. Respondents should be aware that notwithstanding any other provision of law, no person shall be subject to a penalty for failing to comply with a collection of information if it does not display a currently valid OMB control number.</p> <p>PLEASE DO NOT RETURN YOUR FORM TO THE ABOVE ADDRESS.</p>					
1. REPORT DATE (DD-MM-YYYY) March-2004		2. REPORT TYPE Master's Thesis		3. DATES COVERED (From – To) Jun 2003 – Mar 2004	
4. TITLE AND SUBTITLE FORECASTING ADVECTIVE SEA FOG WITH THE USE OF CLASSIFICATION AND REGRESSION TREE ANALYSES FOR KUNSAN AIR BASE				5a. CONTRACT NUMBER	
				5b. GRANT NUMBER	
				5c. PROGRAM ELEMENT NUMBER	
6. AUTHOR(S) Lewis, Danielle M., Captain, USAF				5d. PROJECT NUMBER	
				5e. TASK NUMBER	
				5f. WORK UNIT NUMBER	
7. PERFORMING ORGANIZATION NAMES(S) AND ADDRESS(S) Air Force Institute of Technology Graduate School of Engineering and Management (AFIT/ENP) 2950 Hobson Way, Bldg 640 WPAFB OH 45433-7765				8. PERFORMING ORGANIZATION REPORT NUMBER AFIT/GM/ENP/04-08	
9. SPONSORING/MONITORING AGENCY NAME(S) AND ADDRESS(ES) 8 th Operational Support Squadron Weather Flight (8 OSS/OSW) Unit 2139 APO AE 96264-2139 Captain Marc Hidalgo DSN 315-782-4501				10. SPONSOR/MONITOR'S ACRONYM(S)	
				11. SPONSOR/MONITOR'S REPORT NUMBER(S)	
12. DISTRIBUTION/AVAILABILITY STATEMENT APPROVED FOR PUBLIC RELEASE; DISTRIBUTION UNLIMITED					
13. SUPPLEMENTARY NOTES					
14. ABSTRACT <p>Advective sea fog frequently plagues Kunsan Air Base (AB), Republic of Korea, in the spring and summer seasons. It is responsible for a variety of impacts on military operations, the greatest being to aviation. To date, there are no suitable methods developed for forecasting advective sea fog at Kunsan, primarily due to a lack of understanding of sea fog formation under various synoptic situations over the Yellow Sea. This work explored the feasibility of predicting sea fog development with a 24-hour forecast lead time. Examined in this work were data sets of Kunsan surface observations, upstream upper air data, sea surface temperatures over the Yellow Sea, and modeled analyses of gridded data over the Yellow Sea. A complete ten year period of record was examined for inclusion into data mining models to find predictive patterns. The data were first examined using standard statistical regression techniques, followed by classification and regression tree analysis (CART) for exploring possible concealed predictors. Regression revealed weak relationships between the target variable (sea fog) and upper air predictors, with stronger relationships between the target variable and sea surface temperatures. CART results yielded several relationships between the target variable and upstream upper air predictors, as well as, upstream model analyses over the Yellow Sea. The results of the regression and CART data mining analyses are summarized as forecasting guidelines to aid forecasters in predicting the evolution of sea fog events and advection over the area.</p>					
15. SUBJECT TERMS Sea fog, Classification and Regression Tree, CART, Advection fog, Advective sea fog					
16. SECURITY CLASSIFICATION OF:			17. LIMITATION OF ABSTRACT	18. NUMBER OF PAGES	19a. NAME OF RESPONSIBLE PERSON
a. REPORT	b. ABSTRACT	c. THIS PAGE			Ronald P. Lowther, Lt Col, USAF
U	U	U	UU	103	19b. TELEPHONE NUMBER (Include area code) (937) 255-3636, ext 4645